Cent. Eur. J. Geosci. • 6(4) • 2014 • 565-587
DOI: 10.2478/s13533-012-0196-6

VERSITA

Central European Journal of **Geosciences**

Petrology of potassic alkaline ultramafic and carbonatitic rocks from Planalto da Serra (Mato Grosso State), Brazil

Topical issue

Piero Comin-Chiaramonti[1], Celso B. Gomes[2], Angelo De Min[1], Excelso Ruberti[2]*, Vicente A.V. Girardi[2], Francesca Slejko[1], Renato D. Neder[3], Francisco E.C. Pinho[3]

1 *Department of Mathematics and Geosciences, University of Trieste, Via Weiss 8, I–34127 Trieste, Italy*

2 *Institute of Geosciences, University of São Paulo, Rua do Lago 562, 05508-080 São Paulo, Brazil*

3 *Institute of Geosciences, Federal University of Mato Grosso, Avenida Fernando Corrêa 2367, 78.060-900 Cuiabá, Brazil*

Received 24 October 2013; accepted 20 March 2014

Abstract: The Planalto da Serra igneous rocks form plugs, necks and dykes of carbonate-rich ultramafic lamprophyres (aillikites and glimmerites with kamafugitic affinity) and carbonatites (alvikites and beforsites). Phlogopite and/or tetraphlogopite, diopside and melanitic garnet are restricted to aillikitic rock-types, whereas pyroclore occurs only in carbonatites. Aillikites and carbonatites are altered to hydrotermalites, having chlorite and serpentine as dominant minerals. Planalto da Serra igneous rock association has kamafugitic affinity (i.e. effusive, ultrapotassic. High LREE/HREE fractionation, incompatible elements data and Sr-Nd isotopes, suggest that the K-ultramafic alkaline and carbonatite rocks originated from a variably metasomatized mantle source enriched in radiogenic Sr. Crustal contamination is negligible or absent. Age values of 600 Ma rule out the geochronological relationship between the investigated intrusions and the Mesozoic alkaline bodies from the Azimuth 125° lineament. The TDM model ages allow to conclude that Planalto da Serra magma is derived from the partial melting of a mantle source metasomatised by K-rich carbonatated melt during the Early to Late Neoproterozoic. On the basis of alkaline magmatism repetitions at 600 Ma and 90-80 Ma we question the subsistence of a stationary mantle plume for so long time.

Keywords: alkaline magmatism • aillikite • glimmerite • kamafugite • carbonatite • petrology • geochemistry

1. Introduction

Neoproterozoic rocks are found at the southern margin of the Amazonian Craton. They belong to the Paraguay Belt (PB, Fig. 1A), a tectonic feature crossed by the Azimuth 125° lineament [1, 2], along which some important Brazilian alkaline provinces of the Mesozoic age also occur (Fig. 1B).

The Paraguay Belt is geographically divided by Neogene sediments of the Pantanal Basin into two sectors named the northern and the southern Paraguay Belt. The first sector was developed during the Brasiliano Cycle [8, 9], and the stratigraphy mainly consists of metaepiclastites and low-grade metasedimentary units of the Cuiabá Group

*E-mail: exrubet@usp.br

(850-630 Ma). The lower unit contains metalimestones of the Araras Group (approximately 580 Ma); the upper unit includes low-grade metasedimentary formations of the Alto Paraguay Group (590-545 Ma) [10–12].

More recently, the Paraguayan Belt was interpreted as being linked to the closing of the Goiás-Pharusian Ocean due to successive continental collisions (600-650 Ma), which sutured the West African Craton against the Saharan Metacraton in the north, and the Amazonian against the São Francisco Craton in the south [13]. Several Brasiliano-Pan African orogenic belts were created in this process and are aligned along a very long area of South America and Africa (more than 6000 km long) dominated by one of the major tectonic elements of the world, the Transbrasiliano-Kandi lineament [13].

In particular, at the northeastern side of the northern Paraguay Belt, i.e., in the Planalto da Serra (PdS) region, some K-alkaline ultramafic and carbonatitic rocks occur, intruding low-grade metasedimentary rocks of the Cuiabá Group along the Rio dos Cavalos Rift (Figs. 2 and 3).

2. Geological outlines

The PdS magmatic rocks are located at the central part of the South American Plate, lying NE of the city of Cuiabá, Mato Grosso State (Fig. 2). They are part of the numerous outcropping bodies close to the Azimuth 125° lineament [2], around the margins of the Paraná Basin [16]. These rocks were emplaced during the Late Neoproterozoic and are aligned along a NE-SW trending extensional zone, the Rio dos Cavalos Rift (Fig. 3). This rift was developed between the northeastern part of the Paraná Basin and the southeastern margin of the Amazonian Craton within the Late-Proterozoic Paraguay mobile belt.

The PdS rock types are represented by dykes, plugs and breccia pipes (diatremes) of aillikites and glimmerites (carbonate-rich ultramafic lamprophyres of kamafugitic affinity) and carbonatites. Although the regional metamorphism of greenschist facies, which is estimated to have occurred near the end of the Brasiliano Orogeny (540-520 Ma) [17] or as late as 490 Ma [18], may have changed their original mineralogy, the age of the Planalto da Serra rocks is well constrained at approximately 600 Ma on the basis of Ar-Ar radiometric determinations performed on phlogopite [19].

3. Petrography

Aillikites and glimmerites

Aillikites are represented by ultramafic alkaline dykes and plugs in which phlogopite and/or tetraferriphlogopite are the most abundant minerals (glimmerites if phlogopite > 50 vol. %). They are inequigranular rocks, coarse to fine in texture, having prevailing phlogopite- tetraferriphlogopite (up to 60 vol%) and subordinate amphibole and/or clinopyroxene, magnetite and primary calcite. Clinopyroxene (and sometimes phlogopite) appears partially or completely replaced by amphibole. Accessories include apatite, titanite, perovskite, garnet and pyrite. In some plugs, garnet is an important phase (up to 15 vol%). Chlorite and serpentine may occur as secondary accessories (replacing original olivine). Representative modal results are in Table 1A.

Carbonatites

Carbonatite rock types are represented by calcite-carbonatite (alvikite in texture) and dolomite-carbonatite (beforsite). Alvikite dykes (MT-5) are mainly made up of calcite, and theirs characteristic feature is the granular, hypidiomorphic, medium to fine-grained texture. The other carbonatites (Table 1B) are beforsite breccia pipe, coarse to medium-grained in texture. Beforsites are constituted by predominant euhedral to subhedral dolomites, associated with clasts of quartz and glass. Amphibole, phlogopite, apatite, magnetite, pyrite, perovskite, pyrochlore and titanite are subordinated minerals. In a few samples, chlorite and serpentine pseudomorphs after mafic minerals are also noted. Phlogopite is euhedral, but also forms irregular and interstitial aggregates in contact with opaques and apatite. Perovskite is suhedral and disseminated, but in some samples it is found as irregular aggregates in association with opaques. Chlorite is present as interstitial fibrous aggregates, or as thin (millimetric) veins together with carbonates. Opaques are magnetite and pyrite. Pyrochlore is present in some samples; the grains are brownish, euhedral to subhedral and associated with apatite and opaques. Some dykes are rich in primary carbonate (calcite up to 26 vol%) and have hydrothermalized chilled margins (Table 1C) where clinopyroxene is completely uralitized.

Hydrothermalites

Some samples (MT-9 and MT-10) from the Mutum dyke contain a prevailing hydrothermal association of chlorite-serpentine-carbonate and are here defined as hydrothermalites.

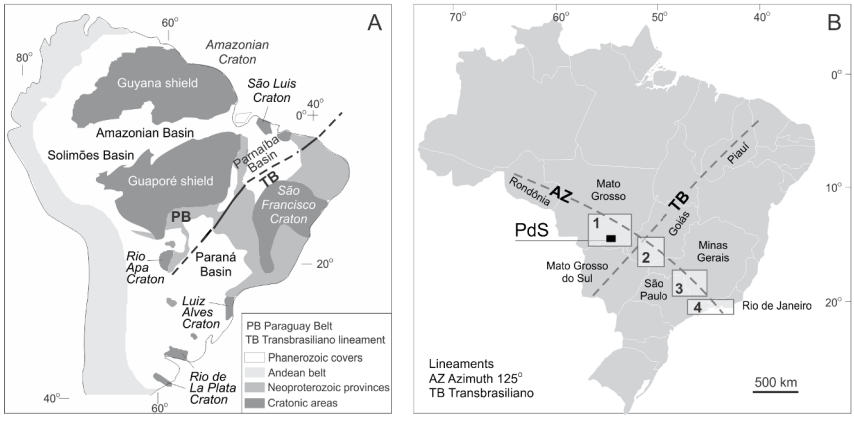

Figure 1. A) Map of South America (modified after [3–5]), showing cratonic areas, Neoproterozoic provinces and Phanerozoic covers. PB, Paraguay Belt; TB, Transbrasiliano huge continental shear zone (or a mega-suture). B) Two main Brazilian lineaments, TB, Transbrasiliano and AZ, Azimuth 125° [1, 2], the latter including the alkaline provinces of: 1, PoxorÃ×u (84 Ma); 2, Rio Verde-Iporá and Goiás (90-80 Ma); 3, Alto Paranaíba (85 Ma); and 4, Serra do Mar (85-55 Ma), according to Gibson et al. (1995, 1997) [6, 7].

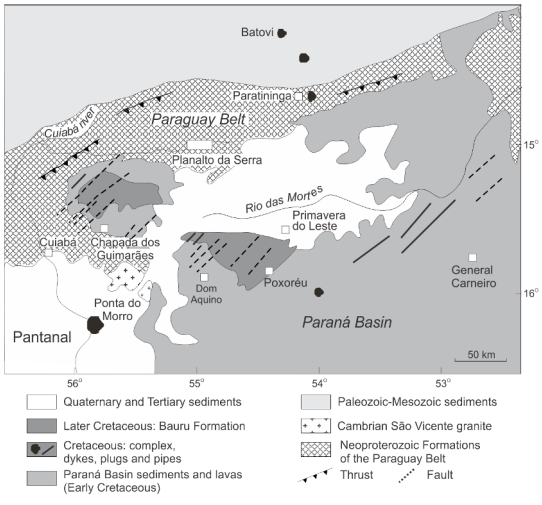

Figure 2. Geological setting showing part of the northern Paraguay Belt and the PdS area [14].

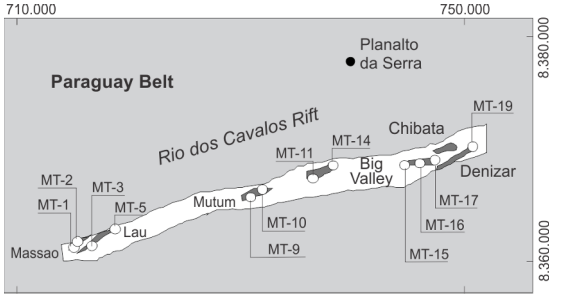

Figure 3. Sketch showing the PdS area and the Rio dos Cavalos Rift in the Paraguay Belt. The location of ultramafic and carbonatitic outcrops [15] and the analyzed samples are indicated.

4. Analytical methods

Microprobe analyses of minerals were carried out at the São Paulo, Modena and Padova Universities, utilizing distinct equipments at each locations: at São Paulo, a Jeol model JXA-8600; at Modena, an ARL-SEMQ; and at Padova, an energy dispersive spectrometer EDS EG 1G connected to a SEM AUTOSCAN microprobe. Chemical analyses of rocks for major elements were performed at the University of Trieste by XRF fluorescence techniques employing a PW1400 automatic spectrometer and pressed-power pellets. FeO analysis was carried out by volumetric titration using ammonium metavanadates, and CO_2 and H_2O were evaluated by wet chemical analyses. Concentrations of trace elements for rocks and carbonate fractions were determined by ICP-mass spectrometer at the Actlabs, Ontario, Canada; Sr and Nd isotopic analyses were performed at the University of Trieste.

5. Mineral chemistry

Phlogopite

Mica is an important mineral of the PdS rocks and it is mainly represented by phlogopite and tetraferriphlogopite. These minerals occur as a primary phase, but can also be found as small aggregates of secondary origin showing chlorite as the most common alteration product.

Table 1. Estimated modal mineral abundances of the main rocks (vol% and calculated out of 1000 counted points; tr=trace) from PdS (see Fig. 3 for localities). Glass*, isotropic material with n < 1.5 (opal?). Cf. Tables A and B of the appendix.

	Aillikitic-Glimmeritic rocks					
	MT-1	MT-2 Dyke Massao	MT-3	MT-15	MT-16	MT-17
Locality	Dyke Massao		Dyke Massao	Plug Chibata	Plug Chibata	Plug Chibata
Phlogopite	50	44	58	51	60	43
Calcite	8	15	6	3	2	12
Dolomite	-		-	-	-	-
Amphibole	24	15	18	-	-	-
Clinopyroxene	4	12	2	22	22	13
Magnetite	8	9	9	15	3	9
Apatite	3	3	3	4	4	4
Garnet	tr	tr	tr	tr	6	15
Titanite	tr	tr	tr	tr	tr	1
Perovskite	tr	tr	tr	1	3	1
Pyrite	tr	tr	1	tr	tr	tr
Chlorite	1	1	2	4	-	-
Serpentine	2	1	1	-	-	-

	Carbonatitic rocks					Hidrothermalites	
	MT-5	MT-11	MT-13	MT-14	MT-19	MT-9	MT-10
Locality	Alvikitic dyke Lau	Beforsitic neck Big Valley	Beforsitic neck Big Valley	Beforsitic neck Big Valley	Beforsitic neck Denizar	Carbonated dyke Mutum	Hydrothermalite dyke margin Mutum
Phlogopite	15	5	-4	3	9	29	3
Amphibole	20				14	24	20
Calcite	51	3			3	26	3
Dolomite	-	59	59	65	51		
Magnetite	4	7	4	10	6	9	8
Pyrite	tr	tr	tr	tr	5	4	4
Apatite	3	1	2	2	2	1	3
Titanite	tr	tr	tr	tr	2	3	2
Perovskite	2	tr	tr	tr	2	tr	1
Chlorite	5	4	2	tr		1	29
Quartz and glass*		15	20	8	4		
Serpentine		6	9	12		3	27
Pyrochlore?	tr	tr	tr	tr	1		

Chemical analyses results are reported in Table 2, with the structural formulae calculated assuming the positive charges balanced on 10 oxygen atoms and 2(OH+F+Cl) atoms; tetrahedral sites are filled by Si, Al or Ti, or by F^{3+} in the case of a deficiency to 4.00 a.f.u. The octahedral sites have Ti, Fe, Mg or Mn, whereas alkalis were assigned to the interlayered positions [20].

Chemical analyses (Fig. 4A) show overlapping compositions for micas from the two main PdS petrographic associations, with the phlogopite from carbonatites tending toward eastonite compositions. In general, early phlogopite progressively grades into tetraferriphlogopite as a result of Al-deficiency during crystallization, a feature also noted in Brazilian alkaline-carbonatitic rocks (e.g., Araxá) [22], kamafugitic and kimberlitic rocks (Alto Paranaíba Province)[23], and Uganda kamafugites [24]. Notably, the MT-9 and MT-10 samples display crystal rims strongly enriched in Ba, most likely due to a highly localized influx of residual oxidized carbonatitic fluid [25].

Carbonates

Carbonate minerals correspond to 2-15 vol% of the whole composition of the glimmerites. Calcite shows low MgO contents and relatively high SrO percentages (0.38-1.52 wt%), whereas dolomite is the main constituent of the beforsitic rocks (Tables 1 and 3). In the MT-5 alvikite, the

Table 2. Representative chemical compositions of phlogopites. Structural formulae on the basis of 24 (O,OH, F) and estimated H_2O assuming (OH, F)=4.000 a.f.u. Analyses from [19] are in italics.

Sample	MT-1	MT-3 Core	MT-3 Rim	MT-5	MT-9 Core	MT-9 Rim	MT-10 Core	MT-10 Rim	MT-16 Core	MT-16 Rim	MT-17	MT-19
SiO_2	38.68	38.97	37.59	36.16	34.17	32.4	35.5	31.08	38.89	37.99	38.96	39.99
TiO_2	1.81	2.82	3.9	0.32	1.17	1.69	0.76	1.97	2.1	2.13	2.18	2.32
Al_2O_3	13.2	12.81	14.09	18.13	16.13	20.5	17.46	17.94	11.55	11.67	11.86	12.35
Fe_2O_3	1.41	1.6	1.19	4.92	0	0	3.01	0	3.65	5.72	4.74	4.86
FeO	9.7	6.09	6.64	1.22	4.03	1.83	3.22	4.62	2.99	0.87	2.17	2.66
MnO	0.21	0.09	0.07	0.1	0.05	0.05	0.16	0.04	0.07	0.06	0.05	0.02
MgO	20.37	22.43	21.83	25.07	24.86	23.82	23.35	23.49	25.17	25.52	24.8	23.7
CaO	0.03	0.03	0	0.07	0.05	0.05	0.18	0.02	0.03	0.04	0.06	0.1
BaO	0	0.54	0.5	0.16	6.66	9.32	1.08	11.18	2.02	1.19	1.33	0.79
Na_2O	0.13	0.04	0.02	0.04	0.06	0.47	0.07	0.15	0.12	0.08	0.13	0.18
K_2O	10.5	10.47	10.1	10.18	8.31	6.83	10.49	5.65	9.77	10.26	9.78	9.3
F	0.21	0.19	0.06	0.12	0.53	0.65	0.36	0.5	1.09	1.51	1.08	0.65
H_2O	3.75	3.91	4.23	3.51	2.98	2.39	4.05	4.36	2.55	3	2.88	3.08
Sum	100	100	100	100	100	100	100	100	100	99.96	100.02	100
a.f.u.												
Si	2.84	2.82	2.72	2.59	2.87	2.44	2.55	2.33	2.72	2.71	2.75	2.82
Al	1.14	1.09	1.2	1.41	1.13	1.56	1.45	1.59	1.2	0.98	1.08	1.05
Ti	0.02	0.09	0.08	0	0	0	0	0.08	0.08	0.23	0.1	0
Fe^{3+}	0	0	0	0	0	0	0	0	0	0.08	0.07	0.13
Sum	4	4	4.00	4	4	4	4	4	4	4	4	4
Al	-	-	-	0.02	0.18	0.16	0.03	0	-	-	-	-
Ti	0.08	0.07	0.13	0.02	0.06	0.09	0.04	0.03	0.13	0	0.08	0.13
Fe^{3+}	0.08	0.1	0.09	0.21	0	0	0.17	0	0.09	0.23	0.15	0.14
Fe^{2+}	0.6	0.38	0.41	0.07	0.23	0.11	0.2	0.31	0.41	0.05	0.21	0.16
Mg	2.23	2.43	2.36	2.67	2.55	2.65	0.01	2.64	2.36	2.72	2.55	2.57
Mn	0.01	0.01	0.01	0.01	0	0	2.55	0	0.01	0	0.01	0
Sum	3	2.99	3	3	3.02	3.01	3	2.99	3	3	3	3
Na	0.02	0.01	0	0.01	0.01	0.07	0.01	0.02	0	0.01	0.01	0.03
K	0.98	0.97	0.93	0.95	0.75	0.66	0.96	0.54	0.93	0.94	0.94	0.95
Ca	0	0	0	0.01	0.01	0	0.01	0	0	0.01	0.01	0.01
Ba	0	0.02	0.02	0.01	0.19	0.27	0.02	0.34	0.02	0.04	0.03	0.02
Sum	1	1	0.95	0.98	0.96	1	1	0.9	0.95	1	0.99	1.01
OH	1.84	1.9	2.04	1.68	1.4	1.2	1.9	2.18	2.04	1.71	1.8	1.64
F	0.05	0.04	0.01	0.04	0.12	0.16	0.25	0.12	0.01	0.34	0.16	0.15
O	10.11	10.06	9.95	10.28	10.48	10.61	9.85	9.7	9.95	9.95	10.04	10.21
Sum	12	12	12	12	12	12	12	12	12	12	12	12

calcite content can reach up to 51%. Other carbonate minerals were not observed. REE carbonates are also present as primary or secondary phases (ΣREE up to 192 ppm in carbonatic phases). Notably, in the MT-19 sample, dolomite (51 vol%) coexists with exsolved calcite (3 vol%).

Clinopyroxenes

Clinopyroxenes are diopsidic in composition (Table 4 and Fig. 4B) and occur only in glimmerites. In dykes (e.g., MT-3), the mineral is found as relict crystals in association with amphibole, phlogopite and carbonates. Cumulus diopside is present in the plugs. In some glimmerites, diopside relicts can be found; however in alvikitic dyke and hydrothermalites, the original clinopyroxene has been

Table 3. Average microprobe analyses of carbonates. CO_2 calculated from stoichiometry. End members in wt% are also reported.

Sample	MT-1	MT-2	MT-3	MT-5	MT-9	MT-10	MT-11
FeO	0.37	0.21	0.19	0.06	0.05	0.37	0.27
MnO	0.17	0.25	0.43	0.16	0.01	0.23	–
MgO	1.22	0.59	0.34	0.22	0.01	0.45	18.84
CaO	52.87	54.19	54.56	55.13	55.69	54.73	33.68
SrO	1.52	1.1	1.23	0.54	0.84	0.38	0.03
BaO	0.05	0.03	0.03	0.02	0.04	0.05	–
CO_2	43.8	43.92	44.09	43.86	44.11	43.98	47.17
Sum	100	100.29	100.87	99.99	100.75	100.19	99.99
End members (wt%)							
Calcite	94.35	96.12	96.53	98.39	98.66	97.49	–
Siderite	0.87	0.74	0.99	0.35	0.08	0.97	–
Magnesite	2.55	1.24	0.7	0.46	0.02	0.94	–
Strontianite	2.17	1.56	1.74	0.77	1.19	0.54	–
Witherite	0.06	0.04	0.04	0.03	0.05	0.06	–
Dolomite	–	–	–	–	–	–	100

Sample	MT-13	MT-14	MT-15	MT-16	MT-17	MT-19	MT-19
FeO	0.27	0.28	0.07	0.22	0.29	0.07	0.29
MnO	0.01	–	0.02	0.13	0.21	0.02	–
MgO	20,35	21.1	0.1	0.28	0.47	0.12	21.85
CaO	31.91	31.02	55.11	55.03	54.53	55.5	30.13
SrO	0.04	0.05	1.34	0.86	0.93	1.34	0.06
BaO	–	–	0.17	0.11	0.04	0.17	–
CO_2	47.43	47.55	44.16	47.68	43.96	44.35	47.68
Sum	100.01	100	100.97	100.01	100.4	101.57	100.01
End members (wt%)							
Calcite	–	–	97.51	97.5	96.92	97.51	–
Siderite	–	–	0.14	0.56	0.67	0.14	–
Magnesite	–	–	0.25	0.58	0.98	0.25	–
Strontianite	–	–	1.88	1.21	1.33	1.88	–
Witherite	–	–	0.22	0.14	0.05	0.22	–
Dolomite	100	100	–	–			100

Table 4. Representative microprobe analyses of clinopyroxenes. Total Fe was partitioned to Fe_2O_3 and FeO assuming charge balance and a theoretical formula containing 4 cations and 6 oxygens.

Sample	MT-1	MT-2	MT-3	MT-15	MT-16	MT-17
SiO_2	55.37	55.41	54.24	55.25	53.82	54.96
TiO_2	0.02	0.22	0.26	0.1	0.08	0.1
Al_2O_3	0.08	0.1	0.35	0.09	0.09	0.09
Cr_2O_3	0.06	0.1	0.06	0.09	0.11	0.09
Fe_2O_3	1.6	0.59	0.78	1.21	1.42	1.2
FeO	–	1.2	1.59	0.4	–	0.4
MnO	0.14	0.1	0.07	0.11	0.09	0.08
MgO	17.95	19.82	17.77	18.65	17.81	18.55
CaO	26.52	22.59	24.66	25.38	26.48	25.24
Na_2O	0.1	0.15	0.09	0.11	0.08	0.11
K_2O	–	0.06	0	0.03	0.02	0.03
Sum	101.83	100.28	99.97	101.41	100	100.05
a.f.u.						
Si	1.974	1.989	1.965	1.963	1.944	1.967
Al^{IV}	0.003	0.004	0.011	0.003	0.004	0.003
Ti	0.001	0.007	0.007	0.003	0.002	0.002
Fe^{3+}	0.043	0	0.017	0.031	0.05	0.028
Sum	2	2	2	2	2	2
Al^{VI}	0	0	0.004	0	0	0
Fe^{2+}	0	0.036	0.033	0.012	0	0.012
Mn	0.004	0.003	0.002	0.003	0.003	0.003
Mg	0.953	1.06	0.959	0.991	0.956	0.99
Fe^{3+}	0.021	0.016	0.029	0.012	0	0.012
Cr	0.002	0.003	0.002	0.002	0.003	0.002
Ca	1.013	0.869	0.965	0.971	1.031	0.971
Na	0.007	0.01	0.006	0.008	0.006	0.008
K	0	0.003	0	0.001	0.001	0.002
Sum	2	2	2	2	2	2
Atoms%						
Ca	50.3	44.2	48.9	48.4	50.5	48.5
Mg	47.3	53.8	48.5	49.4	46.9	49.5
ΣFe+Mn	2.4	2	2.6	2.2	2.6	2

completely substituted by tremolite. Notably, in some carbonatites, clinopyroxene ghosts appear to be completely replaced by amphibole and/or chlorite/serpentine.

Amphiboles

Amphiboles are mainly tremolitic in composition (Table 5) and usually replace the clinopyroxene. Notably, the replacement of anhydrous by hydrous minerals is commonly interpreted as caused by infiltration of a rock by warm H_2O-rich fluids [28], which is also suggested by the textural characteristics of the MT-10 hydrothermalite.

Opaques

Pyrite is a common accessory phase in all of the samples and is an important mineral (content up to 4-5 vol%) in the MT 9 and MT-10 hydrothermalites and in the MT-19 beforsite (Table 1). The mineral most likely represents a later phase, as indicated by the presence of pyrite including titanomagnetite of the same composition as that of the groundmass magnetite (MT-10).

All of the specimens contain titaniferous magnetite (ulvöspinel from 4 mol% to 43 mol%; Tabl 6); the main difference among the specimens is the Cr content (Fig. 5). The Cr/(Cr+Al) ratios are in the range of 0.5-0.9 and 0.0-0.4. Notably, in the MT-5 alvikitic dyke, subordinate

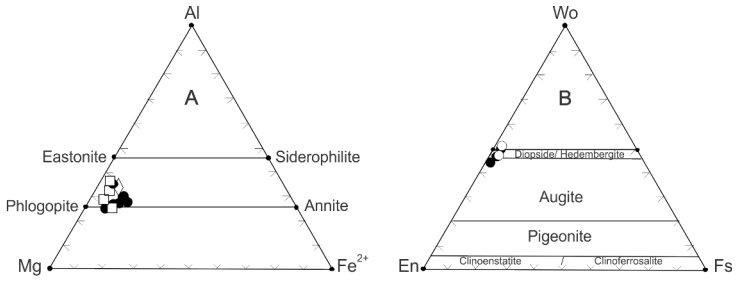

Figure 4. A) Composition of micas on the conventional Al-Mg-Fe diagram [21]. Full circles are glimmerites; open squares are carbonatites; open diamonds are hydrothermalites. B) Clinopyroxene compositions (full circles are dykes; open circles are plugs) on the Wo-En-Fs ternary system. Nomenclature after [26]. Grey areas represent the fields of the APIP kamafugites.

xenocystals rich in spinel (47 mol%) and Mg-chromite (31 mol%, not shown in Fig. 5) are present in addition to the late Ti-magnetite. Occasionally the magnetite is altered into hematite.

Garnet

Garnet is restricted to aillikites-glimmerites and constitutes an important phase only in the Chibata plug (MT16 and MT-17 samples: 6 vol% and 15 vol%, respectively). Crystals are subidiomorphic to idiomorphic and are brownish and fine-grained. The mineral presents a melanitic composition [30] and fits the equilibrium cooling trend at the temperature of 900°C and pressure of 0.2 GPa (Table 7, Fig. 6; [31]).

Alteration products of phlogopite and tremolite

Secondary minerals are mainly represented by chlorite and serpentine (Table 8). They occur as alteration products of phlogopite and tremolite and are particularly abundant in the MT-10 hydrothermalite (29 vol% chlorite, 27 vol% serpentine). Sometimes chlorite and serpentine are found replacing the original phases that have the shape of olivine. According to [32], high calcium contents imply chloritization under high CO_2 activity. The chlorites are compositionally distinctive, high in SiO_2 and MgO and low in Al_2O_3, and they plot inside the field of the chlorites of Sierra Leone kimberlites (Fig. 7). However, the diatreme facies, explosive and H_2O enriched (e.g., MT-10; Table 1), result in the formation of serpentine+chlorite. Moreover, there is also textural evidence of transformation to serpentine with tremolite as a probable precursor.

6. Accessory minerals

Perovskite and Nb-rich oxides

Perovskite microphenocrystals and microlites are ubiquitous and can be an important accessory phase (up to 2-3 vol%; Table 1) in some glimmerites and carbonatites. Representative chemical analyses are reported in Table 9. Applying the oxygen barometer, it is possible to estimate the oxygen fugacity (fO_2) during the crystallization and emplacement of the rocks (ANNO, relative to the nickel-nickel oxide buffer) [34]. The ANNO values obtained for the PdS rocks vary from 0.63 to 2.50. Notably, the Ca/Ti ratios are higher than unity (1.022±0.004 a.f.u.), and some amount of REE (Σ=2.4-4.7 wt%), $(Nb,Ta)_2O_5$ (0.6-0.7 wt%), other than Th (up to 0.60 wt%) and Fe_2O_3 (1.38-1.96 wt%) are present. These results are very similar to those of fO_2 (ANNO) conditions for Lac de Gras pipes [35, 36].

Nb-rich phases are present as accessory microlites (≤1 vol%) in the carbonatite groundmass. Representative chemical analyses relative to MT-5 alvikitic and MT-19 beforsitic samples are listed in Table 9, where the more abundant elements are Nb (Nb_2O_5, 63-65 wt%), CaO (~14 wt%) and Na_2O (~7.4 wt%). On the basis of the Ti-Nb-Ta relationships, these phases can be classified as pyrochlore [37]. Similar compositions are reported by [38] for pyrochlore from Blue River carbonatites in British Columbia.

Titanite and apatite

Titanite and apatite are ubiquitous accessory minerals and occur as microlites and rarely as microphenocrystals. The major element contents in titanite are relatively constant, specifically SiO_2=29.8±0.3 wt% wt%, TiO_2=36.2±0.5 wt%, CaO=26.1±0.3 wt% (Table 10).

In apatite, the following ranges of F and Sr contents were detected: F, 3-4.7 wt%; and Sr, <0.1-0.3 wt%. Notably, these variations closely match those registered in apatites from Leucite Hills [39] and Paraguay [16].

Table 5. Representative microprobe analyses of amphiboles. Fe^{3+} and Fe^{2+} are repartitioned according to [27]. Structural formulae are calculated on the basis of 24(O,OH,F) and H_2O is estimated assuming (OH,F)=2.000 a.f.u.

Sample	MT-1	MT-2	MT-3	MT-5	MT-9	MT-10	MT-19
SiO_2	57.42	57.36	57.7	56.97	56.43	57.68	57.24
TiO_2	0.05	0.05	0.02	0.08	0.06	0.03	0.05
Al_2O_3	0.4	0.23	0.15	0.15	1.22	0.6	0.5
Fe_2O_3	1.24	0.91	1.48	0	1.16	0.43	0.86
FeO	1.78	2.44	2.51	3.03	4.03	1.53	2.58
MnO	0.13	0.16	0.18	0.16	0.25	0.2	0.18
MgO	23.04	23.08	22.98	23.22	21.41	23.31	22.79
CaO	13.63	13.38	13.64	12.87	12.79	12.67	13.12
Na_2O	0.2	0.2	0.19	0.21	0.27	0.28	0.23
K_2O	0.12	0.09	0.08	0.07	0.06	0.04	0.07
F	0.17	0.1	0.06	0.08	0.06	0.04	0.08
Cl	0.01	0.01	0	0	0.01	0.01	0.01
Sum	98.09	98.01	98.81	96.84	97.68	96.82	97.71
a.f.u.							
Si	7.869	7.903	7.865	7.975	7.885	7.947	7.908
Al	0.065	0.031	0.002	0.025	0.115	0.053	0.052
Ti	0.005	0.009	0.024	0	0	0	0.006
Fe^{3+}	0.061	0.057	0.109	0	0	0	0.034
Sum	8	8	8	8	8	8	8
Al	0	0	0	0	0.075	0.006	0.016
Ti	0	0.003	0	0.008	0.006	0.003	0.003
Fe^{3+}	0.067	0.037	0.044	0	0.061	0.045	0.042
Fe^{2+}	0.204	0.199	0.267	0.127	0.373	0.177	0.228
Mg	4.714	4.743	4.668	4.846	4.454	4.785	4.692
Mn	0.015	0.018	0.021	0.019	0.031	0.015	0.019
Sum	5	5	5	5	5	5	5
Fe^{2+}	0	0.019	0.019	0.039	0.036	0	0.019
Na	0	0.01	0	0.031	0.052	0.078	0.032
Ca	2.001	1.974	1.99	1.93	1.912	1.87	1.941
Sum	2.001	2.003	2.009	2	2	1.948	1.992
Na	0.053	0.043	0.05	0.026	0.021	0	0.03
K	0.023	0.017	0.014	0.013	0.011	0.008	0.013
Sum	0.084	0.6	0.064	0.039	0.033	0.008	0.043

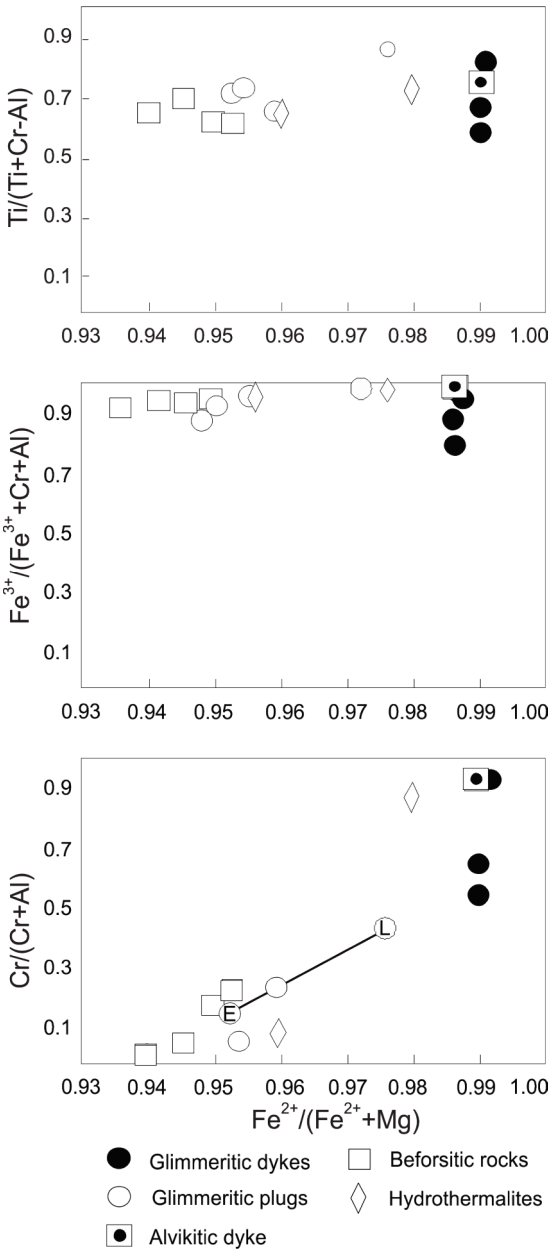

Figure 5. $Fe^{2+}/(Fe^{2+}+Mg)$ versus Ti/(Ti+Cr+Al), $Fe^{3+}/(Fe^{3+}+Cr+Al)$ and Cr/(Cr+Al) planes trough the spinel prism [30] illustrating magnetite variations in the PdS specimens (Table 6). E and L, early and late crystallization, respectively.

7. Significance of the mineralogy

The mineralogy of the PdS rocks, when compared to other alkaline occurrences from the Azimuth 125° lineament (Fig. 1B), is, to some extent, similar to that of the Late Cretaceous kamafugites-glimmerites and carbonatites from APIP described by [6, 7, 40] for the following reasons: 1) an abundance of phlogopite, primary carbonates (aillikites, glimmerites, sÃjvites and beforsites, after [41]) and olivine; and 2) compositions of diopside, phogopite (tetraferriphlogopite), carbonates, opaques (titanomagnetite and chromium-spinel) and accessory apatite, titanite, perovskite and pyrochlore [42, 43]. The presence of primary melanitic garnet is indicative of equilibrium at 900°C and 2-5 Kb pressure [31]. However, the presence of the tremolitic amphibole may be associated with hydratation, nucleation and growth of amphibole, followed

Table 6. Representative microprobe analyses of opaques. Fe_2O_3 and FeO (wt%) and ulvöspinel (mol%) are calculated according to [29] and end-members are calculated by stoichiometry.

Sample	MT-1	MT-2	MT-3	"MT-5 Early"	"MT-5 Late"	"MT-9 "	MT-10	MT-11
SiO_2	0.18	0.23	0.28	0.17	0.17	0.13	0.23	0.33
TiO_2	11.8	10.9	10	1.03	4.02	0.98	4.52	8.07
Al_2O_3	2.52	1.3	0.07	31.37	0.08	0.03	1.38	2.73
Cr_2O_3	4.43	3.24	2.05	32.31	1.1	0.28	0.15	0.02
FeO_{tot}	73.7	77.36	81.02	17.25	83.76	89.7	85.98	82.26
MnO	2.51	2.03	1.55	0.25	0.53	0.19	0.16	0.13
MgO	0.25	0.22	0.19	16.82	0.22	0.4	0.82	1.23
ZnO	1.48	0.75	0.01	0.1	0.06	0.02	0.01	0.01
Sum	96.87	96.03	95.17	99.3	90.94	91.73	93.25	94.78
Fe_2O_3	36.39	41.69	46.99	0.56	56.69	65.5	57.56	49.9
FeO	40.95	39.84	38.72	16.74	32.74	30.75	34.18	37.35
Sum	100.51	100.2	99.86	99.35	96.61	98.28	99.01	99.77
a.f.u.								
Si	0.053	0.069	0.085	0.039	0.053	0.041	0.071	0.103
Ti	2.638	2.463	2.288	0.18	0.938	0.23	1.054	1.892
Al	0.883	0.454	0.025	8.606	0.029	0.011	0.504	1.002
Cr	1.041	0.773	0.505	5.947	0.27	0.069	0.037	0.004
Fe^{3+}	8.138	9.448	10.758	0.098	13.95	15.382	13.429	11.697
Fe	10.179	10.016	9.852	3.248	8.503	8.025	8.49	8.693
Mn	0.631	0.515	0.399	0.049	0.14	0.05	0.034	0.034
Mg	0.111	0.098	0.086	5.816	0.102	0.186	0.378	0.572
Zn	0.326	0.164	0.002	0.017	0.014	0.005	0.003	0.002
Sum	24	24	24	24	23.999	23.999	24	23.999
Mole%								
Ulvöspinel	43.03	40.95	38.87	3.65	20.69	4.97	19.41	32
Magnetite	39.98	46.96	53.94	-	74.74	91.76	75.83	61.47
Gahnite	3.46	1.74	0.02	0.19	0.17	0.07	0.03	0.02
Spinel	1.18	0.65	0.11	47.36	-	-	2.86	5.34
Hercynite	0.06	0.03	-	-	-	-	-	-
Chromite	5.55	3.71	1.87	31.14	1.58	-	-	-
Mg-chromite	-	0.41	0.83	17.12	-	0.42	0.63	0.03
Jacobsite	6.74	5.55	4.36	0.54	1.19	0.92	0.39	0.37
Mg-ferrite	-	-	-	-		1.86	0.85	0.77

Sample	MT-13	MT-14	MT-15	"MT-16 Early"	"MT-16 Late"	MT-17	MT-19
SiO_2	0.29	0.3	0.3	0.06	0.51	0.31	0.32
TiO_2	6.36	7.21	6.48	11.03	0.34	8.45	7.85
Al_2O_3	1.95	2.34	1.74	2.47	0.02	2.12	2.15
Cr_2O_3	0.76	0.71	0.75	0.57	0.02	0.29	0.1
FeO_{tot}	84.02	83.54	83.82	74.76	91.47	80.71	83.97
MnO	0.73	0.3	0.13	5.27	0.32	2.49	0.45
MgO	0.97	1.1	0.87	0.96	0.42	0.98	1.25
ZnO	0.01	0.03	0.13	0.26	0	0.14	0.03
Sum	95.09	95.53	95.36	95.38	93.1	95.49	96.12
Fe_2O_3	53.79	51.78	53.13	44.51	67.19	35.69	37.17
FeO	35.6	36.95	36.06	34.7	31.01	50.03	51.86
Sum	100.66	100.72	100.73	99.83	99.83	100.5	101.18

Table 6. Contd.

a.f.u.							
Si	0.087	0.089	0.091	0.018	0.156	0.092	0.094
Ti	1.43	1.61	1.472	2.478	0.078	1.893	1.755
Al	0.686	0.819	0.619	0.87	0.007	0.744	0.726
Cr	0.181	0.167	0.18	0.135	0.005	0.068	0.023
Fe^{3+}	12.098	11.57	12.076	10.011	15.518	11.216	11.542
Fe	8.899	9.176	9.108	8.67	7.959	8.892	9.189
Mn	0.185	0.075	0.033	1.334	0.083	0.628	0.113
Mg	0.432	0.487	0.392	0.427	0.192	0.435	0.551
Zn	0.002	0.007	0.029	0.057	0	0.031	0.007
Sum	24	24.001	24	24	23.998	23.999	24
Mole%							
Ulvöspinel	25.96	28.65	26.69	40.4	4.35	33.12	30.98
Magnetite	66.97	64.95	68.15	39.9	92.27	54.71	61.6
Gahnite	0.02	0.07	0.33	0.63	-	0.34	0.07
Spinel	3.9	4.54	3.19	4.1	0.04	3.8	4.2
Hercynite	-	-	-	-	-	-	-
Chromite	-	-	-	0.48	-	-	-
Mg-chromite	1.04	0.94	1.03	-	0.03	0.38	0.13
Jacobsite	2.11	0.85	0.37	14.49	1.02	6.99	1.26
Mg-ferrite	-	-	0.24	-	2.29	0.66	1.76

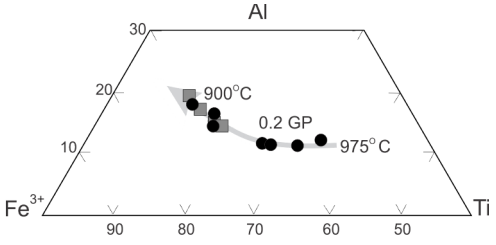

Figure 6. Compositions of melanitic garnets (grey squares) from PdS rocks, as represented on the Al-Fe^{3+}-Ti triangular plot (atom%, cf. Table 7). Temperatures (°C) and equilibrium cooling trends at 0.2 GPa are after [31].

by continuous dissolution of diopside at 800-850°C (approximately 5 Kb; [28, 44, 45]). Finally, hydrothermal alteration affecting the pre-existing parageneses is responsible for the formation of chlorite, serpentine and pyrite. Notably, chorite and serpentine appear as pseudomorph of olivine.

8. Petrochemistry

The aillikites-glimmerites (Table 11, with the wt% of major oxides recalculated on a water-free basis) fit the kamafugitic field of [46] and/or the TAT (Toro-Ankole type) and II fields of [47] (Fig. 8). The glass in the MT-3 beforsitic neck also shows a kamafugitic affinity.

It is interesting to note that, on the basis of the above classification, the PdS samples refer specifically to rocks defined as ultrapotassic (i.e., K_2O/Na_2O>2 wt%, K_2O>3 wt% and MgO>3 wt%), plotting into the Toro Ankole Group (Group II of [47]) and that the carbonatites can be considered strongly potassic to some extent, having K_2O/Na_2O ratios of 14.4±12.3 and K_2O of 1.38±0.15 wt%. The variation diagrams of MgO vs. major oxides (Fig. 9) confirm the kamafugitic affinity of the non-carbonatitic samples.

Additionally, the pairs of major and trace elements of the glimmerites exhibit ranges for incompatible elements in or near the kamafugitic fields. In particular, there are apparent correlations between Nd and Sm, Th and U, La and Yb and Sr and Rb (Fig. 9); however, correlations are not as evident for the carbonatites (Table 12). For the aillikitr-glimmerites, the Zr vs. Cr diagram defines a liquid with an initial Zr content of approximately 240 ppm, which is similar to the lower limit of thr APIP lithotypes (cf. Fig. 4 of [41]), suggesting a comparable mantle source and comparable melting degrees.

Incompatible elements, normalized to a primitive mantle composition (Fig. 10A), show different behaviors for both petrographic associations and single occurrences. In fact, the glimmerites, the MT-5 alvikite and the hydrothermalites that display a kamafugitic affinity are characterized by negative anomalies in K, Sr-P, Hf and Ti, and

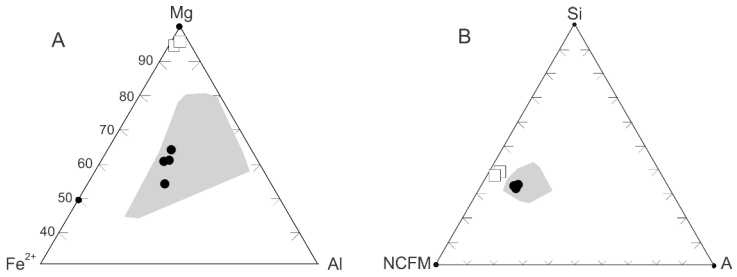

Figure 7. A) Chlorite analyses plotted as a function of Mg-Fe^{2+}-Al. B) Si-NCFM (Fe^{2+}+Mg+Mn+Ca+2Na+2K-Ti)-A(Al+ Fe^{3+}+Cr+2Ti) diagram after [33]. Field variation of kimberlitic chlorites from Sierra Leone is also shown (grey fields; [32]). Full circles are chlorites; open squares are serpentines.

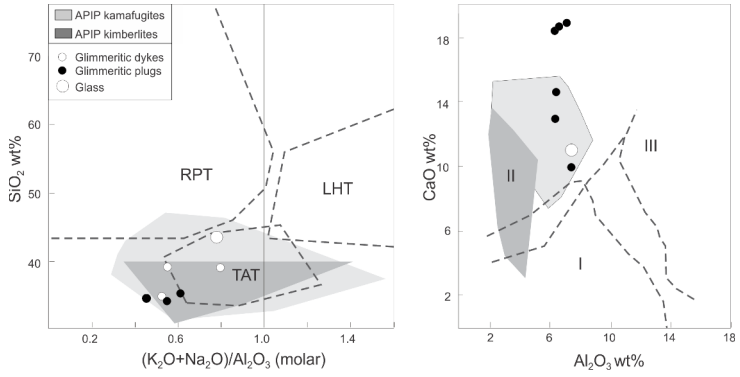

Figure 8. PdS rocks: molar $(K_2O+Na_2O)/Al_2O_3$ versus SiO_2 (wt% on a water-free basis: LHT, Leucite Hills; TAT, Toro-Ankole; RPT, Roman Province lavas type after [46] and CaO vs. Al_2O_3 (Group I, LHT; Group II, TAT; Group III, RPT; after [47]) diagrams. APIP kamafugite and kimberlite fields are after [41].

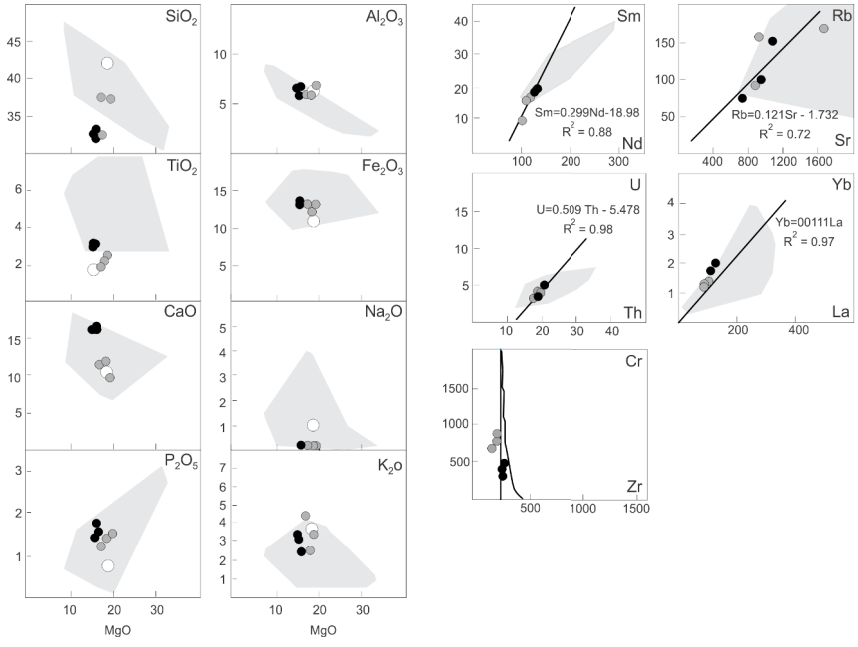

Figure 9. MgO versus major oxides and trace elements for the silicate rocks from Planalto da Serra (grey fields are APIP kamafugites). In the Zr versus Cr diagram, the heavy line represents the liquid descent of the APIP rock types (Zr_0=240; lower limit of Fig. 4 in [41]). Symbols are the same as in Fig. 8.

Table 7. Representative microprobe analyses of garnets. Structural formulae on 24 oxygen basis and Fe_2O_3 as from charge balance.

Sample	MT-1	MT-15	MT-16	MT-17
SiO_2	30.76	33.17	33.21	33.14
TiO_2	6.71	4.74	5.66	3.82
Al_2O_3	3.35	3.78	3.31	4.23
Cr_2O_3	0.25	0.07	0.05	0.06
Fe_2O_3	27,36	24.33	24.34	24.32
MnO	1.18	1.21	1.26	1.18
MgO	0.18	0.23	0.19	0.25
CaO	29.82	32	32.19	31.8
Na_2O	0.19	0.05	0	0.09
Sum	99.8	99.58	100.21	98.89
a.f.u.				
Si	5.195	5.554	5.529	5.579
Al	0.667	0.446	0.471	0.421
Ti	0.139	0	0	0
Sum	6	6	6	6
Al	0	0.299	0.179	0.418
Ti	0.713	0.597	0.709	0.484
Cr	0.033	0.009	0.007	0.008
Fe^{3+}	3.254	3.065	3.049	3.081
Sum	4	3.97	3.944	3.991
Fe^{2+}	0.223	0	0	0
Mn	0.169	0.174	0.178	0.169
Mg	0.045	0.06	0.047	0.063
Ca	5.496	5.74	5.742	5.738
Na	0.062	0.015	0	0.03
Sum	5.967	5.989	5.967	6
Al	16.9	16.9	14.7	19
Fe^{3+}	69.6	69.6	69.2	70
Ti	13.5	13.5	16.1	11

Table 8. Representative microprobe analyses of chlorites (a.f.u. on the basis of 28 O), and of serpentines (a.f.u. on the basis of 7 O).

0	MT-3	MT-5	MT-10	MT-11	Serpentine	MT-10	MT-11
SiO_2	32.65	31.91	33.3	32.23	SiO_2	41.3	41.69
TiO_2	0.21	0.15	0.2	0.31	TiO_2	0.06	0.07
Al_2O_3	9.13	8.74	9.32	8.99	Al_2O_3	0.55	0.57
FeO	18.98	22.69	16.26	17.87	Cr_2O_3	0	0.01
MnO	0.06	0.06	0.05	0.06	FeO	3.34	3.6
MgO	26.91	24.39	29.49	27.05	MnO	0.03	0.03
CaO	0.17	0.23	0.15	0.15	MgO	40.2	39.53
Na_2O	0.01	0.02	0	0.02	CaO	0.16	0.13
K_2O	0.12	0.04	0.15	0.12	Na_2O	0	0.01
Sum	88.24	88.23	89.1	86.8	K_2O	0.02	0.03
					NiO	0.01	0.01
					Sum	85.67	85.68
a.f.u.					a.f.u.		
Si	6.611	6.613	6.597	6.598	Si	1.971	1.989
Al	1.389	1.387	1.403	1.402	Al	0.029	0.011
Sum	8	8	8	8	Sum	2	2
Al	0.79	0.742	0.777	0.768	Al	0.002	0.021
Ti	0.032	0.024	0.03	0.048	Ti	0.002	0.003
Fe_2+	3.226	3.909	2.717	3.061	Cr	0	0.001
Mg	8.139	7.534	8.659	8.258	Fe_2+	0.133	0.144
Mn	0.007	0.007	0.006	0.011	Mg	2.862	2.813
Sum	12.194	12.215	12.189	12.146	Mn	0.001	0.001
					Na	0	0.001
Na	0.004	0.01	0	0.007	K	0.001	0.002
K	0.03	0.011	0.038	0.032	Ca	0.008	0.007
Ca	0.037	0.051	0.034	0.033	Ni	0	0.001
Sum	0.071	0.072	0.072	0.072	Sum	3.009	3

positive anomalies in Th, La, Nd, Eu and Tb. Ba and Rb show either negative or positive anomaly. However, the beforsites exhibit strong negative Rb-Ba anomalies and relative enrichment in Th, U, K, La and Ce.

The chondrite-normalized REE distribution (Fig. 10B) displays behaviors similar to strong LREE/HREE fractionation, specifically $(La/Yb)_c$: 65.0±1.3 (aillikite-glimmerite dykes), 56.6±2.2 (aillikite-glimmerite plugs), 90.3±8.7 (hydrothermalites), 56.1±11.7 (beforsites), 76 (MT5 alvikite), and 40.3±6.9 (carbonate fraction of MT-3 and MT-5 samples). These latter MT-3 and MT-5 samples also show Eu/Eu* (Sm-Gd normalization) negative anomalies, specifically 0.29 (MT-3) and 0.47 (MT-5), probably due to a previous crystallization of Ca-rich phases (possibly clinopyroxene-amphibole). Alternatively, this behavior could be related to the country rock during the hydrothermal event.

Considering the high MgO contents, up to 19 wt% in the aillikites and glimmerites, the REE distribution most likely represents the products of partial melts of a veined mantle source, strongly enriched in incompatible elements and C, H (e.g., phlogopite-amphibole-carbonate-rich veins; [41]).

9. Isotopic systematics

A complete discussion regarding the age of rocks intruding this tectonic feature is provided by [19]. The following is a summary of the main points: $^{40}Ar/^{39}Ar$ (phlogopite and tetraferriphlogopite) yielded an age of approximately 600 Ma (averaging 602±16 Ma); and Rb/Sr systematics, relative to the MT-19 beforsite (whole rock, carbonate fraction and insoluble residue), define an isochron Rb/Sr of 598±10 Ma, similar to the Sm/Nd age (errorchron for all

Table 9. Representative analyses of perovskites. Structural formulae on 3 oxygen basis. ΔNNO: oxygen barometer after Bellis and Canil (2007). The composition of Nb-rich oxides is also shown (pyrochlore?).

Sample	MT-5	MT-15	MT-16	MT-19	*a.f.u.*	MT-5	MT-15	MT-16	MT-19	"Nb-rich oxides"	MT-5	MT-19
SiO_2	0.12	0.06	0	0.26	Si	0.003	0.001	0	0.006	Nb_2O_5	65.53	63.27
TiO_2	52.19	53.63	55.07	54.29	Ti	0.926	0.938	0.95	0.942	Ta_2O_5	3.43	5.69
Th_2O	0.6	0.35	0.11	0.09	Th	0.007	0.004	0.001	0.001	TiO_2	1.56	2.15
Al_2O_3	0.31	0.3	0.3	0.29	Al	0.009	0.008	0.008	0.008	Th_2O	0.51	0.46
Fe_2O_3	1.96	1.67	1.38	1.51	Fe^{3+}	0.034	0.029	0.023	0.026	UO_2	0.02	2.16
Nb_2O_5	1.43	1	0.55	0.69	Nb	0.015	0.011	0.006	0.007	La_2O_3	0.17	0.11
Ta_2O_5	0.25	0.17	0.09	0.12	Ta	0.002	0.001	0	0.001	Ce_2O_3	0.26	0.26
MnO	<0.01	0.01	0.01	0.02	Mn	0	0	0	0	Y_2O_3	0.17	0.13
MgO	0.01	0.01	0.01	0.03	Mg	0	0	0	0.001	FeO	0.03	0.06
CaO	37.26	38.37	39.47	39.2	Ca	0.942	0.957	0.971	0.967	CaO	14.73	14.3
SrO	0.6	0.58	0.57	0.47	Sr	0.008	0.008	0.008	0.006	SrO	0.72	0.63
Na_2O	0.3	0.15	0.2	0.22	Na	0.014	0.011	0.009	0.01	PbO	0	0.03
La_2O_3	1	0.79	0.57	0.58	La	0.009	0.007	0.005	0.005	Na_2O	7.46	7.43
Ce_2O_3	2.42	1.9	1.37	1.39	Ce	0.021	0.016	0.012	0.012	F	5.5	4.66
Pr_2O_3	0.24	0.19	0.13	0.18	Pr	0.002	0.001	0.001	0.001	Sum	100.09	101.34
Nd_2O_3	0.82	0.65	0.48	0.65	Nd	0.007	0.005	0.004	0.005	O=F	2.32	1.96
Sm_2O_3	0.18	0.18	0.19	0.23	Sm	0.002	0.002	0.002	0.002	Sum	96.91	98.64
Sum	99.69	100.01	100.5	100.19	Sum	2.001	1.999	2	2			
					ΔNNO	0.63	1.57	2.5	1.88			

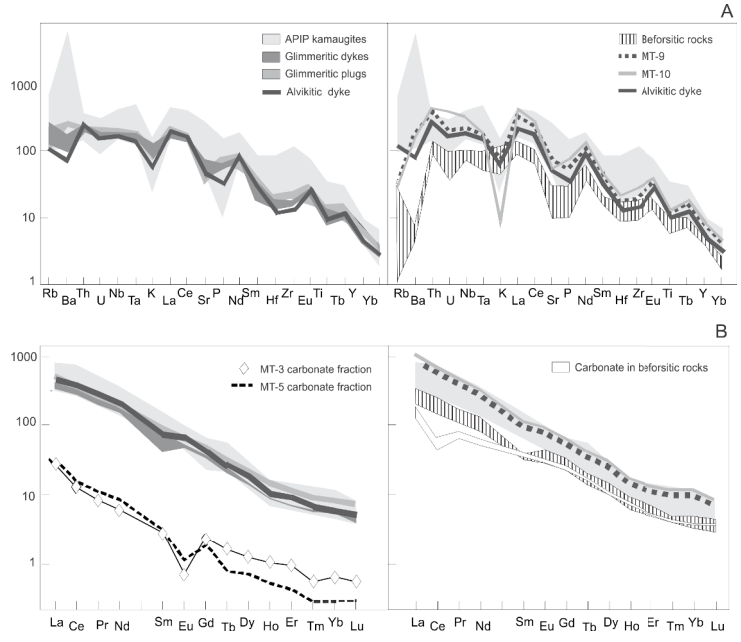

Figure 10. A) Incompatible elements normalized to primitive mantle concentrations (after [48]). B) Chondrite-normalized (after [49]) REE distribution for the various rocks from the PdS region. Data sources in Tables 11 and 12.

the samples) of 601±73 Ma. Notably, new data relative to the Rb/Sr systematic (Table 13A, B), excluding MT-10 hydrothermalite and MT-16 carbonate fraction, give an age of 594±21 Ma (Fig. 11), confirming the previous determinations of [19]. Thus, based on the available data, the K-alkaline-carbonatitic rocks of the Rio de Cavalos Rift have an age of approximately 600 Ma, indicating that this event is associated with the Brasiliano Cycle [13].

Table 10. Representative microprobe analyses of titanites (a.f.u. on the basis of 4Si), and apatites: a.f.u. on the basis of 26(O,F).

Titanite	MT-1	MT-9	MT-10	MT-17	Mt-19	Apatite	MT-1	MT-5	MT-15	MT-19
SiO_2	29.66	30.23	29.53	29.77	30	SiO_2	0.37	0.53	0.12	0.42
TiO_2	35.8	36.96	35.74	36.08	36.54	TiO_2	0.01	0.02	0	0.01
ZrO_2	0	0.02	0.1	0.03	0.04	Al_2O_3	0.28	0.42	0.09	0.33
Nb_2O_5	0.39	0.57	0.72	0.52	0.59	MgO	0.01	0	0.01	0
Al_2O_3	2.15	2.14	2.37	2.2	2.2	CaO	54.55	53.89	55.44	54.33
Fe_2O_3	3.91	3.11	3.2	3.53	3.21	MnO	0.03	0.03	0-02	0.03
MnO	0.05	0.09	0.03	0.05	0.07	FeO	0.33	0.49	0.13	0.38
MgO	0.96	0.78	0.91	0.9	0.83	SrO	0.2	0.3	0.07	0.24
CaO	25.96	26.63	25.89	26.11	26.38	Na_2O	0.08	0.12	0.03	0.1
SrO	0.12	0.26	0.16	0.17	0.22	K_2O	0.01	0.01	0	0.01
Na_2O	0.1	0.06	0.08	0.08	0.07	P_2O_5	42	42	42	42
La_2O_3	0.18	0.37	0.11	0.21	0.29	F	4.36	4.67	3.03	4.28
Ce_2O_3	0.44	0.54	0.28	0.42	0.46	Sum	102.23	102.48	100.94	102.13
Sum	99.86	101.76	99.12	100.07	100.9	O=F	1.84	1.97	1.66	1.88
a.f.u.						Sum	99.71	99.78	99.57	99.73
Si	4	4	4	4	4					
Al	0.171	0.167	0.189	0.175	0.173	P	5.97	5.975	5.965	5.972
Fe^{3+}	0.198	0.155	0.163	0.178	0.161					
Ti	3.631	3.678	3.641	3.645	3.664	Ti	0.001	0.002	0	0.001
Zr	0	0.001	0.007	0.002	0.002	Al	0.056	0.084	0.019	0.202
Sum	4	4.001	4	4	4	Mg	0.001	0	0.001	0
						Ca	9.814	9.692	9.965	9.775
Mg	0.193	0.154	0.184	0.181	0.165	Mn	0.004	0.004	0.002	0.004
Nb	0.012	0.021	0.022	0.017	0.02	Fe	0.032	0.068	0.013	0.05
Mn	0.006	0.01	0.003	0.006	0-008	Sr	0.02	0.03	0.007	0.023
Na	0.013	0.008	0.01	0.011	0.009	Na	0.027	0.041	0.011	0.032
La	0.004	0.009	0.003	0.005	0.007	K	0.001	0.001	0	0.001
Ce	0.011	0.013	0.007	0.011	0.011	Sum	9.956	9.892	10.017	10.088
Sr	0.009	0.02	0.013	0.013	0.017					
Ca	3.751	3.772	3.758	3.758	3.766	F	2.316	2.484	2.091	2.371
Sum	3.999	4.007	4	4.002	4.003					

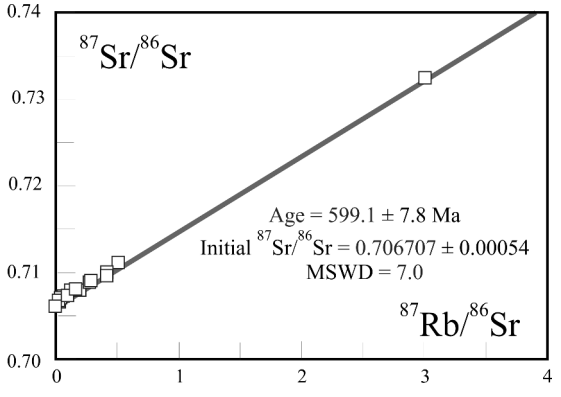

Figure 11. Errorchron relative to the new data of $^{87}Rb/^{86}Sr$ versus $^{87}Sr/^{86}Sr$ from PdS rocks (Table 13B), excluding the samples MT-10 and MT-16 (carbonate fraction).

Sr-Nd isotopes

In general, the high concentration of most incompatible elements (I.E.) in all of the PdS rocks indicates that the effects of crustal contamination on the Nd isotopic systems were negligible and that the parental magma compositions are more likely linked to mantle-enriched sources related to variable degrees of metasomatism (veined mantle). The data are plotted in Fig. 12 (time-integrated ε-notations of Table 13B), with the values concentrated in the enriched quadrant, and with εNd=0.41±0.05 and εSr extending from 4 to 32-41. Notably, the lowest Sr values refer to the MT-10 hydrothermalite and to the carbonate component (Sr=195 ppm) of a glimmeritic plug (εSr wr=32) suggesting a reopening of the system by less enriched fluids, rather than by a selective crustal contamination.

Table 11. Chemical analyses of PdS rocks. Glass is taken from the microprobe analyses. Glimm.= glimmerites. Data from [19] are in italics.

Sample/	MT-1	MT-2	MT-3	MT-15	MT-16	MT-17	MT-13
Locality	Massao	Massao	Massao	Chibata	Chibata	Chibata	Glass
Rock	Aillikitic	Aillikitic	Glimmeritic	Glimmeritic	Glimmeritic	Aillikitic	In beforsitic
type	dyke	dyke	dyke	plug	plug	plug	neck
SiO_2	37.58	32.44	37.36	33.72	32.65	32.13	42.21
TiO_2	1.72	2.49	3.06	3.09	2.99	3.2	1.46
Al_2O_3	6.09	5.96	6.84	5.95	6.62	6.23	7.05
Fe_2O	2.15	1.86	2.04	1.93	2	2.09	3.33
FeO	9.83	9.28	10.2	9.63	10	10.45	6.84
MnO	0.2	0.2	0.18	0.21	0.18	0.23	0.15
MgO	17.26	18.46	19.13	15.88	15.45	16.05	18.55
CaO	12.42	13.57	8.52	17.58	17.61	17.72	10.39
Na_2O	0.13	0.05	0.05	0.23	0.04	0.04	1
K_2O	4.31	2.5	3.41	3.07	3.27	2.57	3.59
P_2O_5	1.2	1.33	1.45	1.75	1.45	1.53	0.76
S	0.09	0.03	0.54	0.04	0.04	0.06	-
CO_2	4	5.04	2.18	2.28	1.07	1.99	-
H_2O^+	2.41	4.86	3.12	4.4	5.04	5.49	-
Sum	99,28	98.07	98.08	99.76	98.41	99.78	95.33
CIPW Norm							
or	-3.63	-	20.15	-	-	-	0.01
ab	-	-	0.42	-	-	-	-
an	3.31	8.65	8.37	6.2	8.23	9.23	4.15
ne	0.6	0.23	-	1.95	0.18	0.18	4.58
lc	17.12	11.59	-	14.23	-	-	16.63
kp	-	-	-	-	10.98	8.79	-
di	20.16	12.15	8.47	5.47	14.08	14.21	33.58
ol	33.71	37.05	38.72	34.88	31.42	32.77	27.02
cs	-	2.53	-	14.73	14.02	12.13	-
mt	3.12	2.7	2.96	2.8	2.9	3.03	4.83
il	3.27	4.73	5.81	5.87	5.68	6.08	2.77
pr	0.19	0.06	1.15	0.08	0.09	0.13	-
ap	2.78	3.08	3.36	4.05	3.36	3.54	1.76
cc	9.1	11.46	4.96	5.19	2.43	4.23	-

Sample	MT-5	MT-11	MT-13	MT-14	MT-19	MT-9	MT-10
Locality	Lau	Big Valley	Big Valley	Big Valley	Denizar	Mutum	Mutum
Rock	Alvikitic	Beforsitic	Beforsitic	Beforsitic	Beforsitic	Carbonataded	Hydrotherm
type	dyke	neck	neck	neck	neck	dyke	dyke
SiO_2	22.05	25.3	27.08	11.87	31.18	27.08	36.16
TiO_2	2.23	1.79	1.19	1.51	2.1	2.61	2.83
Al_2O_3	5.15	1.82	1.63	3.94	3.46	5.79	4.07
Fe_2O3	1.42	0.97	0.77	1.21	1.34	1.76	6.01
FeO	7.08	4.85	3.83	5.56	6.67	9.79	10.41
MnO	0.15	0.24	0.15	0.19	0.13	0.19	0.09
MgO	11.02	12.59	13.82	17	11.74	15.75	26.71
CaO	25.22	21.03	19.52	22.48	17.89	18.47	8.11
Na_2O	0.15	0.05	0.1	0.31	0.7	0.02	0.07
K_2O	1.92	1.61	1.35	1.31	1.45	2.41	0.28
P_2O_5	0.74	0.23	0.64	0.55	0.62	1.31	1.77

Table 11. Contd.

Locality	Lau	Big Valley	Big Valley	Big Valley	Denizar	Mutum	Mutum
Rock	Alvikitic	Beforsitic	Beforsitic	Beforsitic	Beforsitic	Carbonataded	Hydrotherm
type	dyke	neck	neck	neck	neck	dyke	dyke
S	0.02	-	0.03	0.02	2.55	0.97	0.09
CO_2	17.34	28.9	27.85	32.3	18	8.21	1.39
H_2O^+	5.29	0.55	1.15	1.56	1.93	5.42	2.21
Sum	99.78	99.93	99.11	99.81	99.76	99.78	100.17
CIPW Norm							
Q	-	16.3	16.65	-	9.92	-	-
C		-	-	-	0.01	-	-
or	11.34	9.51	7.98	4.08	8.57	-	1.65
ab	0.02	0.43	0.18	-	5.92	-	0.59
an	7.71	-	0.01	5.82	1.98	8.59	9.97
ne	0.68	-	-	1.42	-	0.09	-
lc	-	-	-	2.56	-	11.17	-
di	2.35	-	3.88	3	18.76	2.21	7.83
hy	-	4,32	5.24	-	-	-	17.44
ol	24.9	-	-	8.16	-	34.89	39.05
cs	-	-	-	-	-	6.13	-
mt	2.68	1.41	1.12	1.75	1.94	2.55	8.71
il	5.53	3.4	2.26	2.87	3.99	4.96	5.37
pr	0.06	-	0.06	0.04	5.41	2.06	0.19
ap	2.25	0.53	1.48	1.27	1.44	3.03	4.1
cc	17.86	3.23	-	-	-	18.67	3.16
dolomite	-	57.6	58.36	67.68	37.72	-	-

The isotopic systematics have a distribution that appears distinct from the distribution corresponding to the APIP kamafugites, as indicated in Fig. 12.

Moreover, the almost constant behavior of the Sm/Nd ratio in the rocks (0.13±0.003; Fig. 9 and Tabl 13) suggests that the Nd model ages [19] could be indicative of the main metasomatic event affecting the lithospheric sources beneath the PdS region. These ages (calculated in relation to the depleted mantle, TDM, Table 13; [51]) for the whole PdS population (12 samples) are 1.05±0.08 Ga, which is similar to those calculated for the APIP kamafugites, i.e., TDM=0.97±0.09 Ga (44 samples, cf. inset of Fig. 12) and the Rio Verde-Iporá alkaline province (0.99±0.10 Ga, inset of Fig. 7 of [41]), defining an Early Neoproterozoic age.

However, the "uncontaminated trachybasaltic dykes" from the Poxoréu area [7] display TDM=643±52 Ma. Thus, in spite of the different ages among the Rio dos Cavalos Rift lithotypes (approximately 600 Ma) compared to the APIP, Rio Verde-Iporá and Poxoréu rocks (approximately 84 Ma; [6, 7]), the model ages seem to reflect the time of the event when the fluids were "extracted", metasomatizing the lithospheric mantle.

10. Concluding remarks

Along the Azimuth 125° lineament, where alkaline occurrences are found in many places (Fig. 1B), the Rio dos Cavalos Rift, in the PdS region, is intruded by dykes and necks of ultramafic and carbonatitic rocks within an extensional zone in the Late-Proterozoic Paraguay mobile belt (Cuiabá Group; Fig. 2). The PdS lithotypes are represented by ultrapotassic rocks with kamafugitic affinity, by carbonatitites having alvikitic and beforsitic characteristics and by rocks displaying evidence of late hydrothermalization. These processes, which are responsible for the lowest isotopic Sr values, suggest that the system was partially reopened by a successive event with less enriched fluids.

The PdS lithologies present petrochemical features similar to those from the Late Cretaceous alkaline rocks from the APIP region. However, they yielded similar Ar/Ar, Rb/Sr and Sm/Nd ages of approximately 600 Ma. Notably, the 600 Ma date represents an Ediacaran age (630-542 Ma), at the eastern margin of the Amazonian Craton that was fragmented at the beginning of the Neoproterozoic time [13].

Table 12. Concentrations of trace elements of PdS rocks. Data from [19] are in italics.

Sample	MT-1	MT-2	MT-3	MT-3	MT-5	MT-5	MT-9	MT-10	MT-11
ppm	Massao	Massao	Massao	CF	Lau	CF	Mutum	Mutum	BigValley2
Cr	753	664	816	-	876	-	342	274	144
Ni	628	575	689	-	601	-	359	328	153
Co	86.3	76	94	-	76.4	-	72.4	71.5	26
V	269	147	236	-	161	-	166	125	33
Ba	723	970	1348	809.5	541	503	1488	1220	51
Cs	19.2	24	63.9	16.8	2.6	0.61	1.2	2	<0.1
Rb	58.5	187.6	169.7	1.675	71.9	1.6	21.8	18	18.3
Sr	909	1652	940	6310	1069	2732	1665	1219	200
Zr	215	169.9	210	<0.03	159.4	<0.03	220.4	314.3	95.4
Hf	4.8	4.2	6	-	3.9	-	5.8	7.1	2.5
Nb	140.3	130.9	124.1	<0.01	137.9	<0.01	182.1	252.1	56.2
Ta	8.2	6.9	6.7	-	6.2	-	7.7	8.5	2.2
Y	19	21.7	21.1	3.74	24.2	2.08	36.7	36.6	21.9
U	4.2	4.3	3.4	0.68	3.6	0.02	4.7	9.1	0.8
Th	19.1	19.4	17.7	<0.01	23.4	<0.01	38.2	40.9	8.3
Pb	12.7	7	8.2	2.96	1.6	<0.02	6.1	8.9	4
Cu	72.6	68.7	89.2	-	72.7	-	93.9	113.9	19.7
As	2.9	1	7.5	-	<0.5	-	15	1.8	0.8
Zn	49	62	86	-	27	-	138	99	49
Ga	14.7	12	13.5	-	11.7	-	12.5	13.9	8.2
La	118.1	136.9	117.4	8.86	149.5	10.57	248.1	316.2	91.4
Ce	252.8	286	243.5	11.45	307.9	13.05	448.9	546.5	147.5
Pr	27.53	31.82	26.75	1.09	33.87	1.44	46.69	54.55	17.45
Nd	105.7	118.9	101.1	3.82	126.5	5.36	165.4	194.7	61.9
Sm	15.42	16.23	8.7	0.58	15.09	0.62	23.29	20.27	8.97
Eu	4.15	4.31	3.91	0.06	4.9	0.09	6.3	6.62	2.51
Gd	10.66	10.24	8.96	0.68	12.19	0.51	15.34	16.64	6.43
Tb	1.23	1.21	1.06	0.08	1.36	0.04	1.77	2	0.78
Dy	5.31	5.18	5.14	0.44	6.18	0.24	8.3	9.29	3.87
Ho	0.73	0.77	0.73	0.085	0.81	0.04	1.21	1.26	0.58
Er	1.69	1.68	1.63	0.22	2.01	0.1	2.71	2.96	1.44
Tm	0.22	0.24	0.21	0.02	0.23	0.01	0.34	0.38	0.19
Yb	1.23	1.39	1.24	0.15	1.32	0.065	1.99	2.21	1.06
Lu	0.14	0.19	0.17	0.02	0.17	0.01	0.24	0.27	0.15

Sample	MT-11	MT-13	MT-14	MT-15	MT-16	Mt-16	MT-17	MT-19	MT-19
(ppm)	CF	Big Valley 1	Big Valley 2	Chibata	Chibata	CF	Chibata	Denizar	CF
Cr	-	164	205	390	383	-	417	301	
Ni	-	140	232	368	343	-	364	270	
Co	-	40.2	30.3	66.7	62.9	-	73.8	45.8	
V	-	43	43	97	113	-	276	167	
Ba	27.4	123	49	1893	1941	28.5	1859	629	140
Cs	0.055	0.2	0.1	3	1.9	-	4.7	1	0.06
Rb	0.45	0.4	18.2	75.5	153	0.15	99.3	18.5	0.46
Sr	194	242	195	739	1067	195	933	628	618
Zr	<0.03	115.4	148.4	232.6	236.5	-	267.3	203.5	<0.03
Hf	-	3	3.9	5.9	6.5	-	6.9	5.1	-

Table 12. Contd.

Sample (ppm)	MT-11 CF	MT-13 Big Valley 1	MT-14 Big Valley 2	MT-15 Chibata	MT-16 Chibata	Mt-16 CF	MT-17 Chibata	MT-19 Denizar	MT-19 CF
Nb	<0.01	67.4	80	143.7	136	-	153.5	77.7	0.01
Ta	-	2.6	3.1	7.6	7.3	-	8.1	4.5	-
Y	20	25.9	20.6	31.2	29.9	21	33.2	16.5	15
U	0.12	0.9	1.4	4	3.9	0.13	4.8	2.1	0.31
Th	0.41	9.6	13.1	18.4	18.3	0.39	20.2	8.1	0.4
Pb	1.93	7.5	3.6	1.5	12	1.89	9.9	5.5	2.41
Cu	-	25.8	24.4	87	30.8	-	54.9	66.3	-
As	-	15.4	41.9	-	<0,5	-	2.4	2	-
Zn	-	44	69	61	90	-	104	77	-
Ga	-	6.2	12.3	13.7	13		13.6	11.1	-
La	59.05	68.3	106.9	156.7	150	60	160.5	63	40.91
Ce	55.95	130.5	198.9	311.3	295.2	66.5	318.8	122.1	46.32
Pr	10.3	14.66	21.98	34.28	32.24	-	34.56	13.94	8.22
Nd	40.6	53.8	81.2	126.4	119.9	54.8	128.8	50.5	33.12
Sm	7.93	7.95	6.78	18.62	17.55	8.02	18.73	7.78	6.84
Eu	2.48	2.28	3.47	5.1	4.8	2.51	5.16	2.24	2.21
Gd	6.99	5.76	8.89	12.77	12.5	7.17	13.4	5.81	6.32
Tb	0.885	0.72	1.04	1.56	1.5	-	1.65	0.72	0.81
Dy	3.88	3.39	4.96	7.55	7.1	3.93	7.65	3.57	3.59
Ho	0.61	0.47	0.69	1.13	1.07	-	1.15	0.54	0.57
Er	1.26	1.14	1.6	2.55	2.43	1.28	2.79	1.37	1.2
Tm	0.15	0.15	0.18	0.32	0.3	-	0.36	0.18	0.14
Yb	0.84	0.74	1.11	1.82	1.75	0.85	2	1.09	0.82
Lu	0.13	0.1	0.14	0.23	0.24	-	0.25	0.14	0.12

Table 13. A) Rb and Sr contents (ppm), and $^{87}Rb/^{86}Sr$ and $^{87}Sr/^{86}Sr$ isotopic ratios for the PdS rocks. R0=initial $^{87}Sr/^{86}Sr$ ratios calculated at 600 Ma. WR=whole rock; Cc=calcite; IR=insoluble residue; Dol=dolomite; Cc Fr=carbonate fraction. B) Sm and Nd contents (ppm), and $^{147}Sm/^{144}Nd$ and $^{143}Nd/^{144}Nd$ isotopic ratios for the same samples. Isotopic ratios used: NBS987: $^{87}Sr/^{86}Sr$=0.710250 (2σ: 0.000008) n=20; La Jolla: $^{143}Nd/^{144}Nd$=0.511853 (2σ: 0.000015), n=21. In italics: A, Rb/Sr systematics (MT-19), B, Sm/Nd systematics, data from [19].

A	Rb	Sr	$^{87}Rb/^{86}Sr$	$^{87}Sr/^{86}Sr$	Rock type	Carbonate vol%	R_0 600 Ma
MT-1 WR	58.5	909	0.1862	0.708281 (22)	Aillikitic dyke	8 Cc	0.706688
MT-3 WR	169.7	940	0.5225	0.711106 (24)	Glimmeritic dyke	6 Cc	0.706635
MT-3 Cc Fr	1.675	6310	0.0768	0.707289 (21)			0.706632
MT-5 WR	71.9	1069	0.1946	0.708294 (25)	Alvikitc dyke	51 Cc	0.706628
MT-5 Cc Fr	1.6	2732	0.0017	0.706643 (24)	Alvikitc dyke		0.706629
MT-9 WR	21.8	1665	0.0379	0.707102(25)	Carbonatated dyke	26 Cc	0.70678
MT-10 WR	18	1219	0.0427	0.704668 (21)	Hydrothermalite	3 Cc	0.704302
MT-11 WR	18.3	200	0.2648	0.708965 (24)	Beforsitic neck	59 Dol, 3 Cc	0.7067
MT-11 Dol+Cc Fr	0.045	194	0.00067	0.706707 (25)			0.706701
MT-14 WR	18.2	195	0.2701	0.709164 (25)	Beforsitic neck	65 Dol	0.706853
MT-16 WR	153	1067	0.415	0.709829 (24)	Glimmeritic plug	2 Cc	0.706278
MT-16 Cc Fr	0.15	195	0.0022	0.704525 (23)	Glimmeritic plug		0.704506
MT-16 IR	171	1053	0.47	0.710310 (32)	Glimmeritic plug		0.706289
MT-19 Dol+Cc Fr	0.3	1526	0.0006	0.706731 (22)	Beforsitic neck	51 Dol, 3 Cc	0.706726
MT-19 IR	30.6	29.3	3.029	0.732567(20)			0.70665
MT-19 WR	18.5	628	0.0852	0.707450 (20)			0.706721

Table 13. Contd.

B	Sm	Nd	$^{147}Sm/^{144}Nd$	143Nd/144Nd	Initial 600 Ma	T^{DM}	εSr	εNd
MT-1 WR	15.42	105.7	0.08818	0.512233(21)	0.511886	1071	38.2	0.42
MT-3 WR	8.7	101.1	0.05202	0.512093(20)	0.51189	967	37.4	0.47
MT3 Cc Fr	0.58	3.82	0.09178	0.512249(20)	0.51189	1082	37.4	0.46
MT-5 WR	15.09	126.5	0.07211	0.512172(22)	0.51189	1017	37.3	0.47
MT5 Cc Fr	0.62	5.36	0.06992	0.512163(25)	0.51189	1011	37.3	0.46
MT-9 WR	23.29	165.4	0.08511	0.512219(21)	0.51188	1062	39.4	0.39
MT-10 WR	20.27	194.7	0.06293	0.512133(21)	0.51188	995	4.3	0.41
MT-11 WR	8.97	61.9	0.0876	0.512229(24)	0.51188	1071	38.3	0.39
MT-11 Cc Fr	7.93	40.6	0.11807	0.512353(25)	0.51189	1207	38.3	0.47
MT-14 WR	6.78	81.2	0.05047	0.512084(23)	0.51188	966	40.5	0.4
MT-16 WR	17.55	119.9	0.08848	0.512231(19)	0.51188	1076	32.3	0.36
MT-16 Cc Fr	8.02	54.8	0.08847	0.512227(20)	0.51188	1080	7.2	0.28
MT-19 WR	7.78	50.5	0.09313	0.512250(20)	0.51188	1092	38.6	0.38
						1054±64		

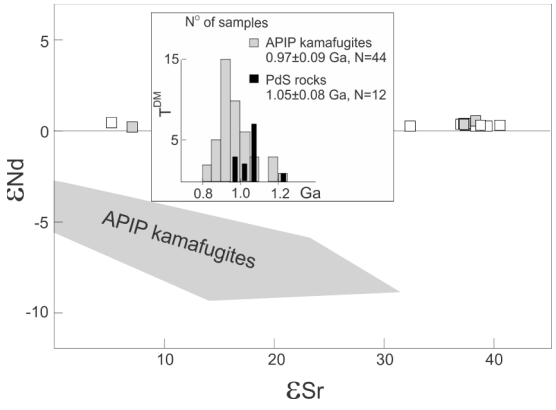

Figure 12. Time integrated, ε notations, $^{87}Sr/^{86}Sr$ (εSr) versus $^{144}Nd/^{143}Nd$ (εNd) correlation diagrams. Open squares are PdS samples (grey squares are carbonate fractions; Table 13). The grey field represents the composition of APIP kamafugites [41]. Inset: histogram relative to Nd model ages (TDM) for the APIP kamafugites (grey) and for PdS samples (black); TDM values: calculation of model dates relative to a depleted reservoir, $^{143}Nd/^{144}Nd$=0.513114 and $^{147}Sm/^{144}Nd$=0.222 [50, 51].

As matter of fact, according to [53], the final amalgamation of Western Gondwana would have occurred at 620 Ma or slightly later, which means that Laurentia, which was still attached to Amazonia, was, for a short time, part of the Gondwana Supercontinent. The opening of the Iapetus ocean characterizes the separation between Laurentia and the Amazonian Craton. It is unknown when this ocean opened, but it could have been just after 600 Ma. Paleomagnetic measurements indicate that the opening occurred at ca. 580 Ma [5].

Taking these factors into account, it is possible that the emplacement of the PdS rocks is related to one of the most important extensional periods of Neoproterozoic times, which is characterized by the separation of Laurentia and the Amazonian Craton [52–54].

Because the Nd model ages (depleted mantle, TDM) are indicative of the main metasomatic events affecting the lithospheric sources beneath the Azimuth 125° lineament, the values of 1.05±0.07 Ga for the PdS population, 0.97±0.09 Ga for the APIP kamafugites and 0.98±0.10 Ga for the Rio Verde-Iporá alkaline volcanics are defining an Early Neoproterozoic age episode, which reflects the time when the fluids metasomatized the lithospheric mantle (cf. also [42]).

In conclusion, the TDM model ages suggest that the PdS magmas were derived from thermal recycling (thermal boundary layer) of the subcontinental lithospheric mantle metasomatised by small-volumes, K-rich carbonatitic melt at the Neoproterozoic, corresponding to the aggregation of the Western Gondwana [52–55].

We consider unlikely that thermal boundary layer activity was due to a permanent plume as proposed by [6]. In alternative we suggest that lithosphere incipient extensional tectonic controlled by an Early Neoproterozoic event, gave rise to similar ultramafic alkaline products at 600 Ma and 90-80 Ma [56, 57]. Notably, a similar case was described by [58] relative.to the genesis of ultramaphic lamprophyres and carbonatites from Ailly Bay, Labrador.

Acknowledgements

The detailed review and helpful suggestions by Francesco Stoppa, Umberto Cordani, Lia Kogarko, Alan Woolley and Gillian Foulger are greatly appreciated. The analytical

support from R. Petrini for isotope analyses and from Sandra Andrade for the chemical analyses of carbonate fractions by ICPM were of great value. The University of Trieste, Italy (grant MIUR-PRIN 2008) and the Brazilian research agency Fapesp (Proc. 10/50887-3, CBG) are acknowledged for their financial support.

Appendix A: Aillikite-gimmerite-carbonatite rock-types from Planalto da Serra (cf. [58], figs. 5 and 6).

II From petrochemical and geochemical points of view, the rock-types from Plalto da Serra fit: The same fields of kamafugites and kimberlites from Alto Paranaiba igneous Province (APIP) (s. Figs 8-9-10 and quoted references).

For these reasons the authors prefer the "kamafugitic affinity".

References

[1] Bardet M.G. 1977. Géologie du diamant. Part 3: gisements de diamants d'Asie, d'Amérique, d'Europe et d'Australasie. Mém. Bureau Réch. Géol. Minières, 1977, 83, 1–169

[2] Biondi J.C., Brazilian mineral deposits associated with alkaline and alkaline-carbonatite complexes. In: Comin-Chiaramonti P., Gomes C.B. (Eds.), Mesozoic to Cenozoic alkaline magmatism in the Brazilian Platform. Edusp/Fapesp, São Paulo, 2005, 707–750

[3] Almeida F.F.M., Hasui Y., O Pré-Cambriano do Brasil. Editora Edgard Blücher, São Paulo, 1984

[4] Heinz M., Debayle E., Vauchez A., 2005. Upper mantle structure of the South American continent and neighboring oceans from surface wave tomography. Tectonophysics, 2005, 406, 115–139

[5] Cordani U.G., Teixeira W., D'Agrella-Filho M.S., Trindade R.I., The position of the Amazonian Craton in supercontinents. Gondwana Res., 2009, 15, 396–407

[6] Gibson S.A., Thompson R.N., Leonardos O.H., Dickin A.P., Mitchell J.G., The Late Cretaceous impact of the Trindade mantle plume: evidence from large-volume, mafic, potassic magmatism in SE Brazil. J. Petrol., 1995, 36, 189–229

[7] Gibson S.A., Thompson R.N., Weska R., Dickin A.P., Leonardos O.H., Late Cretaceous rift-related upwelling and melting of the Trindade starting mantle plume head beneath western Brazil. Contr. Mineral. Petrol., 1997, 126, 303–314

[8] Boggiani P.C., Alvarenga G.J.S., Faixa Paraguay. In: Mantesso-Neto V., Bartorelli A., Carneiro C.D.R., Brito-Neves B.B. (Eds.), Geologia do Continente Sul-Americano: Evolução da obra de F.F.M. de Almeida. Editora Beca, São Paulo, 2004, 3–120

[9] Manzano J.C., Godoy A.M., Araújo L.M.B., Contexto tectÃťnico dos granitóides da faixa de dobramentos Paraguay, MS e MT. Geociências, 2008, 27, 493–507

[10] Lacerda Filho, J.V, Abreu Filho, W., Valente, C.R., Oliveira, C.C., Albuquerque, M.C., Geologia e Recursos Minerais do Estado de Mato Grosso. Programa IntegraÃğão, AtualizaÃğão e Difusão de Dados da Geologia do Brasil. Goiânia, CPRM, 2004

[11] Riccomini C., Nogueira A.C.R., Sial A.N., Carbon and oxygen isotope geochemistry of Ediacaran outer platform carbonates, Paraguay Belt, central Brazil. An. Acad. Brasil. Ci., 2007, 79, 519–527

[12] Alvarenga G.J.S., Boggiani P.C., Babinski M., Dardenne M.A., Figuereido M., Santos R.V., Dantas, E.L. 2010. The Amazonian Palaeocontinent. In: Gaucher C., Sial A.N., Halverson G.P., Frimmel H.E., Neoproterozoic-Cambrian tectonics, global change and evolution: a focus on southwestern Gondwana. Development in Precambrian Geology, 2010, 16, 15–28

[13] Cordani U.G., Pimentel M.M., Araújo C.E.G., Basei A.S., Fuck R.A., Girardi V.A.V., Was there an Ediacaran Clymene Ocean in Central South America? Am. J. Sci., 2013, 313, 517–539

[14] Sousa M.Z.A., Ruberti E., Comin-Chiaramonti P., Gomes C.B., Alkaline magmatism from the Mato Grosso State, Brazil: the Ponta do Morro complex. In: Comin-Chiaramonti P., Gomes C.B. (Eds.), Mesozoic to Cenozoic alkaline magmatism in the Brazilian Platform. Edusp/Fapesp, São Paulo, 2005, 241–260

[15] Ormond M.M.S., Petrografia do complexo alcalino de Planalto da Serra e estudo geológico e geoquímico da intrusão Chibata-Denizar. Laurea Th., Institute of Geosciences, Federal University of Mato Grosso, 2006

[16] Comin-Chiaramonti P., Gomes, C.B. (Eds.), Alkaline magmatism in central-eastern Paraguay. Relationships with coeval magmatism in Brazil. Edusp/Fapesp, São Paulo, 1996

[17] Trindade R.I.F., Font E., D'Agella-Filho M.S., Nogueira A.C.R., Riccomini C., Low-latitude and multiple geomagnetic reversal in the Neoproterozoic Puga cap carbonate, Amazon craton. Terra Nova, 2003, 15, 441–446

[18] Tohver E., Trindade R.I.F., Solum J.C., Hall C.M., Riccomini C., Nogueira A.C., Closing the Clymene ocean

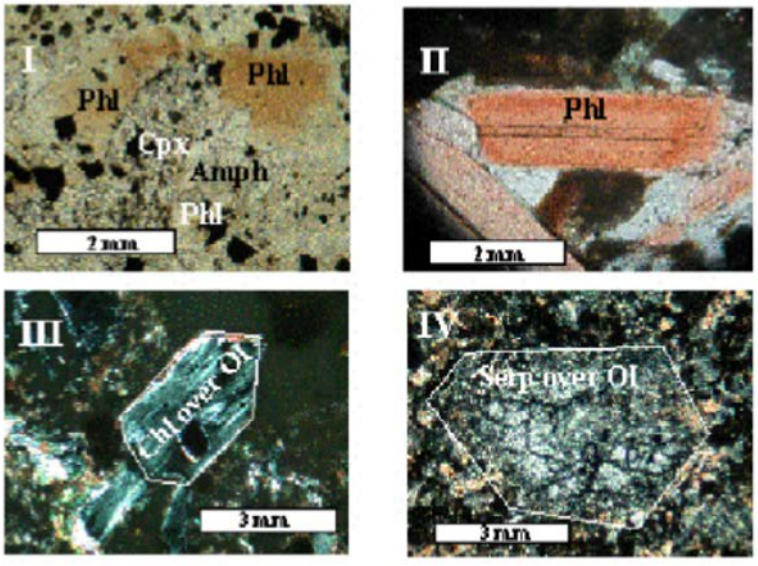

Figure A.1. I. MT-3 aillikitic dyke showing phlogopite (Phl) clinopyroxene (Cpx) partially replaced by amphibole (Amph); N//. II. MT-16 glimmeritic plug characterized by tetraphlogopite (Phl, ~60 vol%); N//. III. MT-15 aillikitic plug plug with relicts of probable olivine (Ol) replaced by chlorite (Chl); N X. IV. MT-1 aillikitic dyke showing relicts of olivine (Ol) completely replaced by serpentine (Serp); N X.

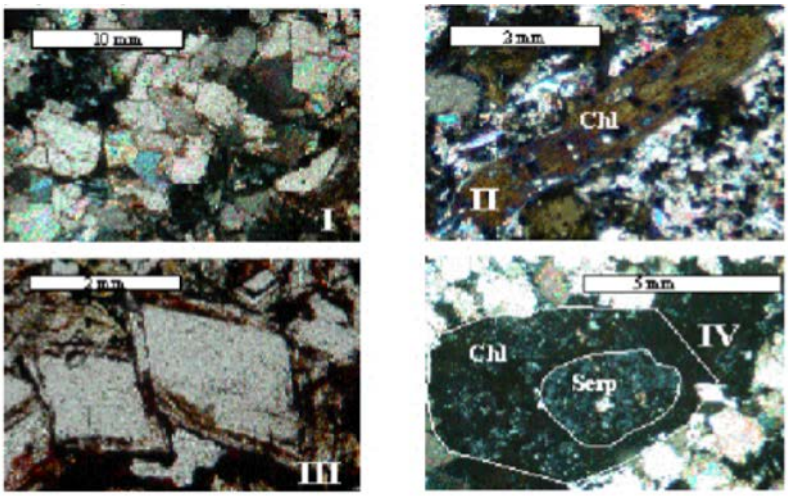

Figure A.2. I. MT-5 alvikite showing the calcite relationships; N X. II. Chlorite (Chl) in MT-5 alvikite; N X. III. MT-11 beforsite showing euhedral dolomite crystals; N//. IV. Chlorite (Chl) and serpentine (Serp) pseudomorphs after mafic minerals in the MT-11 beforsite; N X.

and bending a Brasiliano belt: evidence for the Cambrian formation of Gondwana, southeast Amazon craton. Geol. Soc. Am. Geology, 2010, 38, 267–270

[19] De Min A., Hendriks B.W.H., Slejko F., Comin-Chiaramonti P., Girardi V.A.V., Ruberti E., Gomes C.B., Neder R.D., Pinho F.E.C., Age of ultramafic high-K rocks from Planalto da Serra (Mato Grosso, Brazil). J. South Am. Earth Sc., 2013, 41, 57–64

[20] Brigatti, M.F., Medici, L., Poppi L., Vaccaro C., Crystal chemistry of trioctahedral micas-1M from the Alto Paranaíba Igneous Province, Southeastern Brazil. Can. Mineral., 2001, 39, 1333–1345

[21] Bailey S.W. 1984. Classification and structures of the micas. Crystal chemistry of the true micas. Rev. Mineral., 1984, 13, 1–60

[22] Traversa G., Gomes C.B., Brotzu P., Buraglini N., Morbidelli L., Principato M.S., Ronca S., Ruberti E., Petrography and mineral chemistry of carbonatites and mica-rich rocks from the Araxá complex (Alto Paranaíba Province, Brazil). An. Acad. Brasil. Ci.,

2001, 73, 71–98

[23] Melluso L., Lustrino M., Ruberti E., Brotzu P., Gomes C.B., Morbidelli L., Morra V., Svisero D.P., D'Amelio F., Major- and trace-element composition of olivine, perovskite, clinopyroxene, Cr-Fe-Ti oxides, phlogopites and host kamafugites and kimberlites, Alto Paranaíba, Brazil. Can. Mineral., 2008, 46, 19–40

[24] Scordari F., Schinfaro E., Lacalamita M., Mesto E., Crystal chemistry of trioctahedral micas-2M1 from Bunyaruguru kamafugite (southwest Uganda). Am. Mineral., 2012, 97, 430–439

[25] Kopyloval M.G., Mogg T., Smith B.S., Mineralogy of the Snap Lake kimberlite, Northwest Territories, Canada, and the compositions of phogopite as records of its crystallization. Can. Mineral., 2010, 48, 549–570

[26] Morimoto N., Nomenclature of pyroxenes. Min. Mag., 1998, 52, 535–550

[27] Leake B.E., Nomenclature of amphiboles. Min. Mag., 1998, 42, 533–565

[28] Welch M.D., Pawley R., Tremolite: new enthalpy and entropy data from a phase equilibrium study of the reaction tremolite=2diopside+1.5orthoenstatite+β-quartz+H_2O. Am. Mineral., 1991, 76, 1931–1939

[29] Carmichael I.S.E., The iron-titanium oxides of salic volcanic rocks and their associated ferro-magnesian silicates. Contr. Mineral. Petrol., 1967, 5, 310–357

[30] Deer R.W., Howie R.A., Zussman J., An introduction to the rock-forming minerals. Longman Group UK Limited, London, 1992

[31] Kjarsgaard B.A., Phase relations of a carbonated high-CaO nephelinite at 0.2 and 0.5 GPa. J. Petrol., 1998, 39, 2061–2075

[32] Tomkins L.A., Bailey S.W., Haggerty S.E., Kimberlitic chlorites from Sierra Leone, West Africa: unusual chemistries and structural polytipes. Am. Mineral., 1984, 69, 237–249

[33] Robinson P., Spear F.S., Schumacher J.C., Laird J., Klein C., EVANS B.W., Doolan, B. L., Phase relations of metamorphic amphiboles: natural occurrence and theory. In: Veblen, D.R., Ribbe, P.H. (Eds.), Amphiboles: petrology and experimental phase relations. Mineral. Soc. Am., Rev. Mineral., 1982, 9B, 1–128

[34] Bellis A.J., Canil, D. 2007. Ferric iron in $CaTiO_3$ perovskite as an oxygen barometer for kimberlitic magmas I: experimental calibration. J. Petrol., 2007, 48, 219–230

[35] Chakhmouradian A.R., Mitchell, R.H., Three compositional varieties of perovskite from kimberlites of the Lac de Gras field (Northwest Territories, Canada). Min. Mag., 2001, 65, 133–148

[36] Canil D., Bellis A.J., Ferric iron in CaTiO3 perovskite as an oxygen barometer for kimberlite magmas II: applications. J. Petrol., 2007, 48, 231–252

[37] Černy Y.P., Ercit T.S., Mineralogy of niobium and tantalum. Crystallochemical relationships, paragenetic aspects and their economic implications. In: Moeller P., Èerny P., Sanpe, F. (Eds.), Lantanides, tantalum and niobium. Sp. Publ. Soc. Geol. Applied to Mineral Deposits, 1986, 7, 27–79

[38] Simandl G.J., Jones P.C., Rotella M., Blue river carbonatites, British Columbia. Primary exploration for tantalum. Exploration and Mining in British Columbia, 2001, 123–132

[39] Mitchell R.H., Bergmann S.C. (Eds.), Petrology of lamproites. Plenum Press, New York, 1991

[40] Thompson R.N., Gibson S.A., Mitchell J.G., Dickin A.P., Leonardos O.H., Brod J.A., Greenwood J.C., Migrating Cretaceous-Eocene magmatism in the Serra do Mar Alkaline Province, SE Brazil: melts from the deflected Trindade mantle plume? J. Petrol., 1998, 39, 1493–1526

[41] Gomes C.B., Comin-Chiaramonti P., Some notes on the Alto Paranaíba igneous province. In: Comin-Chiaramonti P., Gomes, C.B. (Eds.), Mesozoic to Cenozoic alkaline magmatism in the Brazilian Platform. Edusp/Fapesp, São Paulo, 2005, 317–340

[42] Bizzi L.A., Araújo, A.L.N. 2005. Dynamics of mantle-derived magmatism in the southwestern São Francisco craton, Brazil. In: Comin-Chiaramonti P., Gomes C.B. (Eds.), Mesozoic to Cenozoic alkaline magmatism in the Brazilian Platform. Edusp/Fapesp, São Paulo, 2005, 341–365

[43] Comin-Chiaramonti P., Gomes C.B., Marques L.S., Censi P., Ruberti E., Antonini P., Carbonatites from southeastern Brazil: geochemistry, O-C, Sr-Nd-Pb isotopes and relationships with the magmatism from the Paraná-Angola-Namibia Province. In: Comin-Chiaramonti P., Gomes C.B. (Eds.), Mesozoic to Cenozoic alkaline magmatism in the Brazilian Platform. Edusp/Fapesp, São Paulo, 2005, 651–682

[44] Jenkins D.M., Holland T.J.B., Clarke A.K., Experimental determination of the pressure-temperature stability field and thermochemical properties of synthetic tremolite. Am. Mineral., 1991, 76, 458–469

[45] Bozhilov K.N., Jenkins D.M., Verben D.R., Pyribole evolution during tremolite synthesis from oxides. Am. Mineral., 2004, 89, 74–84

[46] Barton M., A comparative study of some minerals occurring in K-alkaline rocks of the Leucite Hills, Wyoming, The Vico Volcano, Italy, and Toro-Ankole region, Uganda. Neues Jb. Min. Abh., 1979, 137, 113–134

[47] Foley S.F., Venturelli G., Green D.H., Toscani L., The

ultrapotassic rocks: classification and constraints for petrogenetic models. Earth-Sci. Rev., 1987, 24, 81–134

[48] Sun S.-S., McDonough W.F., Chemical and isotopic systematics of oceanic basalts: implications for mantle composition and processes. In: Saunders A.D., Norry M.J. (Eds.), Magmatism in the ocean basins. Geol. Soc. London, Sp. Publ., 1989, 42, 313–345

[49] Boynton W.V., Cosmochemistry of the Rare Earth elements: meteorite studies. In: Henderson H. (Ed.), Rare Earth Element geochemistry. Elsevier, Amsterdam, 1984, 63–114

[50] Faure G., Principles of isotope geology. John Wiley & Sons, New York, 1986

[51] Dickin A.P., Radiogenic isotope geology, 2nd ed. Cambridge University Press, Cambridge, 2005

[52] Campos Neto M.C., Basei M.A.S., Janasi V.A., Moraes R., Orogen migration and tectonic setting of the Andrelândia Nappe system: an Ediacaran western Gondwana collage, south of São Francisco craton. J. South Am. Earth Sci., 2011, 24, 1–14

[53] Pimentel M.M., Fuck R.A., Jost H., Ferreira Filho C.F., Araújo S.M., The basement of the Brasília Fold Belt and the Goiás Magmatic Arch. In: Cordani, U.G., Milani, E.J., Thomaz Filho, A., Campos, D.A. (Eds.), Tectonic evolution of South America. In: 31st International Geological Congress, Rio de Janeiro, 2000, 195–229

[54] Trompette R., Neoproterozoic (600 Ma) aggregation of Western Gondwana: a tentative scenario. Precambrian Res., 1997, 82, 101–112

[55] Scotese C.R., Late Proterozoic plate tectonics and palaeogeography: a tale of two supercontinents, Rodinia and Pannotia. Geol. Soc. London, Sp. Publ., 2009, 326, 67–83

[56] Ernesto M., Marques L.S., Piccirillo E.M., Molina E., Ussami N., Comin-Chiaramonti P., Bellieni G. Paraná magmatic province - Tristan da Cunha plume systems: fixed versus mobile plume. petrogenetic considerations and alternative heat sources. Journal of Volcanology and Geothermal Researches, 2002, 118, 15–36

[57] De Min A., Comin-Chiaramonti P., Gomes C.B., Girardi V.A.V., Slejko F., Ruberti E. Ultramafic K-alkaline and carbonatitic rocks from Planalto da Serra, Mato Grosso, Brazil. In: http://search.babylon.com/?s=web&babsrc=home&rlz=0&q=Piero+Comin-Chiaramonti&start=10, 2013, 1–23

[58] Tappe, S., Foley S.F., Jenner G.A., Heaman L.M., Kjasgaard B.A., Romer R.L., Stracke A., Joyce, Hoefs J. Genesis of ultramafic lamprophyres and carbonatites at Ailly Bay, Labrador: a consequence of incipient lithospheric thinning beneath the North Atlantic Craton. Journal of Petrology, 2006, 47, 1261–1315